Report Number 97-01

research

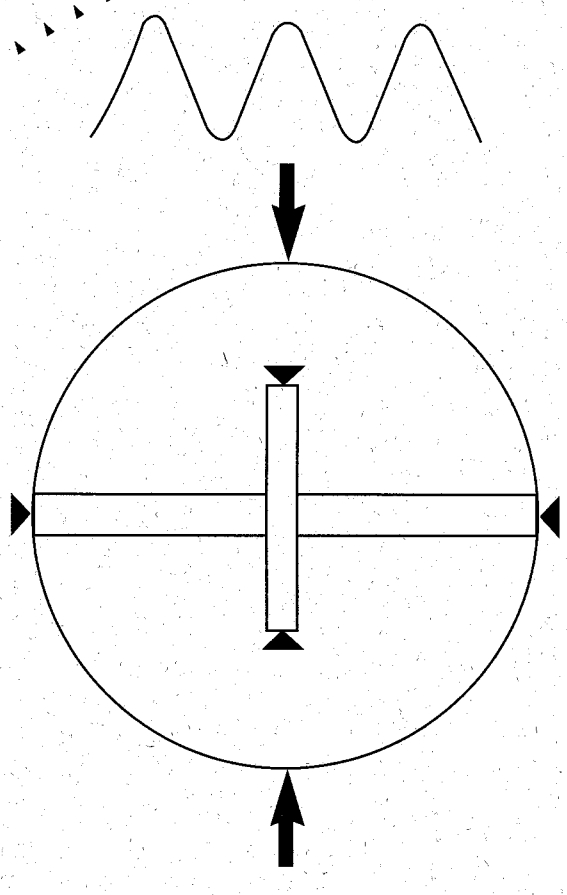

Reassessment of Diametral Compression Test on Asphalt Concrete

UNIVERSITY OF MINNESOTA
CENTER FOR
TRANSPORTATION
STUDIES

Technical Report Documentation Page

1. Report No.	2.	3. Recipient's Accession No.
MN/RC - 97/01		

4. Title and Subtitle	5. Report Date
REASSESSMENT OF DIAMETRAL COMPRESSION TEST ON ASPHALT CONCRETE	December 1996
	6.

7. Author(s)	8. Performing Organization Report No.
Andrew Drescher, David Newcomb and Wei Zhang	

9. Performing Organization Name and Address	10. Project/Task/Work Unit No.
University of Minnesota Department of Civil Engineering 122 CivE Building 500 Pillsbury Dr. S.E. Minneapolis, Minnesota 55455	11. Contract (C) or Grant (G) No. (C) 72273 TOC #147

12. Sponsoring Organization Name and Address	13. Type of Report and Period Covered
Minnesota Department of Transportation 395 John Ireland Boulevard Mail Stop 330 St. Paul, Minnesota 55155	Final Report 1994-1996
	14. Sponsoring Agency Code

15. Supplementary Notes

16. Abstract (Limit: 200 words)

This report examines the diametral compression test, as described in ASTM D4123-82 (1987) and SHRP Protocol P07 (1993) procedures.

The test helps determine the resilient modulus of asphalt concrete, and less frequently its Poisson's ratio, both mechanical parameters of an ideally elastic material.

However, the actual behavior of asphalt concrete is not elastic, but viscoelastic. The viscoelastic behavior of asphalt concrete under traffic-induced loads can be described by the phase angle and the magnitude of the complex compliance or complex modulus. These can be determined from the diametral compression tests that subject the specimen to haversine load history, and from the viscoelastic data interpretation algorithms derived in the current research. To avoid inaccuracies in the data interpretation, the vertical deformation should be measured over a 1/4 diameter central sector of the cylinder by means, for example, of the in-house developed displacement gage.

A series of tests on specimens with various asphalt binder viscosity verified the validity of the viscoelastic data interpretation. Specimens from Mn/ROAD materials showed the presence of viscoelastic properties even at temperatures well below freezing.

17. Document Analysis/Descriptors		18. Availability Statement
Diametral Compression Asphalt Concrete Viscoelastic Properties	Creep Test Haversine Test	No restrictions. Document available from: National Technical Information Services, Springfield, Virginia 22161

19. Security Class (this report)	20. Security Class (this page)	21. No. of Pages	22. Price
Unclassified	Unclassified	90	

REASSESSMENT OF DIAMETRAL COMPRESSION TEST ON ASPHALT CONCRETE

Final Report

Prepared by

Andrew Drescher
David Newcomb
Wei Zhang

University of Minnesota
Department of Civil Engineering
122 CivE Building
500 Pillsbury Dr. S.E.
Minneapolis, MN 55455-0220

December 1996

Published by

Minnesota Department of Transportation
Office of Research Administration
200 Ford Building Mail Stop 330
117 University Avenue
St Paul Minnesota 55155

TABLE OF CONTENTS

List of Figures

List of Tables

Table Page

EXECUTIVE SUMMARY

In recent years, there has been a slow, but gradual, move to the use of more fundamental methods for the design of pavement structures. Concepts of stress and strain are beginning to be used in the pavement design process in the same manner that they would be used for buildings and bridges. This idea requires that the materials be characterized in a way that properties such as the modulus of elasticity or resilient modulus can be estimated. The resilient modulus test for asphalt concrete is currently defined by the ASTM test method D4123 and the SHRP protocol P07. These test methods call for the estimation of resilient modulus using the indirect tension or diametral compression loading. The resilient modulus is used as an input to layered elastic theory in order to calculate the pavement response to load. The problem with this approach is that elastic theory cannot adequately account for the time-dependent (viscoelastic) nature of asphalt mixtures.

The research described herein was originated to use the indirect tension configuration to determine the viscoelastic properties of asphalt mixtures. Thus the sample dimensions and loading equipment remained the same, while extracting more information from the test and appropriately characterizing the material. The loading history was changed by introducing a haversine loading, rather than a pulse/rest time scheme. This simplified the loading history, and made it possible to estimate the viscoelastic parameters. Another justification for determining the viscoelastic properties of asphalt mixtures is that this is how asphalt binders are characterized in the new performance-grading system developed by the Strategic Highway Research Program. The proposed test method would provide information on asphalt mixtures which would be consistent with that provided for the asphalt binders.

The importance of the new test method was illustrated by using it to test Mn/ROAD materials. The results showed that these materials exhibited viscous properties even at temperatures well below freezing.

CHAPTER 1
INTRODUCTION

The design of flexible and rigid pavements is experiencing a transition from empirical or semi-empirical procedures to design methods based on continuum mechanics models. The use of mechanics-based methods requires knowledge of material properties characterizing its deformablity, strength, and fatigue. To determine these properties, tests are required that are sufficiently simple to find wide application, on the one hand, and to simulate the conditions that exist in a pavement structure, on the other. In this report attention is focused on one particular test that has been generally accepted as suitable for determining mechanical properties of asphalt concrete, namely, the diametral compression test.

The objectives of the research described in this report were threefold: 1) to analyze in detail the theoretical solution that forms the basis of the data interpretation of the diametral compression test as recommended in the American Society for Testing and Materials (ASTM) D4123-82 (1987) and Strategic Highway Research Program (SHRP) Protocol P07 (1993) procedures, 2) to derive a solution that incorporates the viscosity of asphalt concrete which is present even at low temperatures, and 3) to analyze improvements in both the measurements and in the interpretation of the test data.

The report is organized in seven chapters. Chapter 1 is an introduction, and Chapter 2 describes the origin and motivation for conducting the diametral compression test. In Chapter 3 the elastic solution by Hondros (1959) which is presently used for data interpretation is analyzed; also, its sensitivity to possible inaccuracies is discussed. Chapter 4 presents a novel, viscoelasticity-based solution of the test. Chapter 5 describes a series of laboratory tests with the aim of illustrating the theoretical analyses presented in Chapters 3 and 4. Chapter 6 includes the data interpretation for evaluating the viscoelastic properties of asphalt concrete, and Chapter 7 summarizes the research effort presenting conclusions and recommendations. More details about the research conducted, theoretical derivations, and data interpretations can be found in Zhang (1996), and Zhang et.al., (1996a, 1996b).

CHAPTER 2
THE DIAMETRAL COMPRESSION TEST

The diametral compression test, also called the indirect tensile test or Brazilian test, was developed independently in Brazil and Japan in the 1940s. The test is done by applying a compressive load to a cylindrical specimen through two diametrally opposite arc-shaped rigid platens. The generalized diametral compression test includes compression of cylinders by three or four loads, diametral compression of spheres, and diametral compression of squares or cubes (Jaeger, 1967). The interest in the diametral compression test stems from the fact that for an elastic material the loading conditions, besides inducing compression, produce a nearly uniform tensile stress over a significant portion of the diametral plane containing the applied load. Because applying a compressive load is technically much easier than tensile, the test became regarded as "ideal" for evaluating the tensile properties of brittle materials such as rock and Portland Cement Concrete (Blakey and Beresford, 1955; Thaulow, 1957; Berenbaum and Brodie, 1959; Fairhurst, 1964; Jaeger, 1967), as well as asphalt concrete (Livneh and Shklarsky, 1962).

Hondros (1959) demonstrated that the test also provides a simple and accurate means for determining elastic properties of Portland Cement Concrete. Extensive laboratory investigations conducted by Hadley et al., (1970), and the fact that a portion of a pavement structure is under tension/compression, validated and promoted wider use of the test for evaluating the elastic properties of asphalt concrete (Schmidt, 1972). As asphalt concrete in pavement systems is exposed predominantly to traffic-induced repeated loads, appropriate test procedures have been developed, and implemented routinely in practice, in which the specimens are subjected to pulse/rest cycles (ASTM D4123-82 (1987), SHRP Protocol P07 (1993)). The results of these tests are used to determine the elastic parameters: Young's modulus, E, and Poisson's ratio, ν; in the pavement literature, the term resilient modulus, and symbol M_R, are traditionally used instead of Young's modulus and symbol E. Accordingly, the test is usually called the resilient modulus test.

In application to asphalt concrete, the elasticity-based interpretation of the diametral compression test is deficient in that it neglects the effect of viscosity that all bituminous materials display to a certain degree. The presence of viscosity manifests itself as time-delayed recovery of deformation in the pulse/rest test recommended for resilient modulus evaluation per ASTM D4123-82 and SHRP Protocol P07 (Fig. 1). Time-delayed recovery is noticeable even at low temperatures, and becomes significant at elevated temperatures. The ASTM D4123-82 and SHRP Protocol P07 account for viscosity in a simplified fashion, by recommending evaluating not only the modulus derived from the pulse (instantaneous modulus), but also the modulus corresponding to the end of a rest period (total modulus). The difference of these two moduli can be regarded as an approximate measure of material viscosity at specified load conditions. Note that in a purely elastic material, no delay of deformation takes place, and only one modulus exists.

This report addresses the issue of asphalt concrete viscosity more rigorously, namely, by deriving an analytic solution for the stresses and strains in the diametral compression test which incorporates the combined effect of elasticity and viscosity within the framework of the theory of linear viscoelasticity. The viscoelastic solution then can be used to determine the viscoelastic properties of asphalt concrete once the deformation of the diametrally compressed cylinder is measured in the test. Although the actual response of asphalt concrete may be non-linear including plastic or viscoplastic effects, the solution presented improves on the elastic solution, and may serve as a reference for more sophisticated analysis.

It is expected that the results presented in this report will stimulate efforts towards establishing experimental methods and guidelines for evaluating the viscoelastic properties of asphalt concrete to complement methods and guidelines presently available for asphalt binders (AASHTO TP 5, in SHRP, 1994).

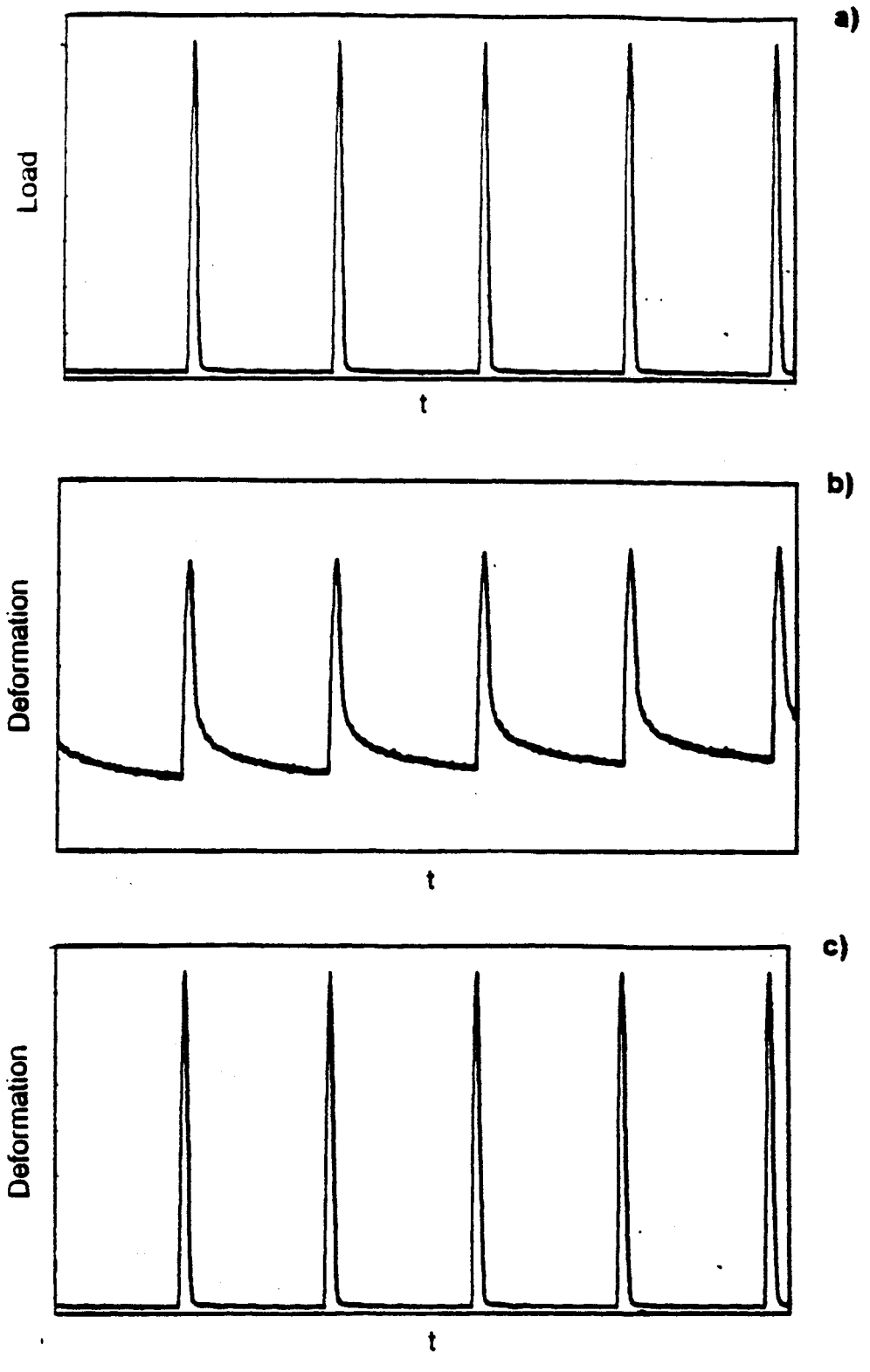

Fig. 1. Pulse-rest test; a) load history, b) deformation in a viscoelastic material c) deformation in an elastic material

CHAPTER 3
ELASTIC SOLUTION

THE ASSUMPTION OF ELASTICITY

The fundamental assumption underlying the interpretation of the diametral compression test according to procedures described in ASTM D4123-82 (1987), and SHRP Protocol P07 (1993), is that the stresses and strains in the cylindrical specimen can be derived from a linear elastic solution. This means that asphalt concrete can be regarded as a linear elastic material, with the stresses and strains satisfying the generalized Hooke's law

$$\varepsilon_{xx} = \frac{1}{E}[\sigma_{xx} - \nu(\sigma_{yy} + \sigma_{zz})] \tag{1a}$$

$$\varepsilon_{yy} = \frac{1}{E}[\sigma_{yy} - \nu(\sigma_{xx} + \sigma_{zz})] \tag{1b}$$

$$\varepsilon_{zz} = \frac{1}{E}[\sigma_{zz} - \nu(\sigma_{xx} + \sigma_{yy})] \tag{1c}$$

$$\varepsilon_{xy} = \frac{1+\nu}{E}\sigma_{xy} \tag{1d}$$

$$\varepsilon_{xz} = \frac{1+\nu}{E}\sigma_{xz} \tag{1e}$$

$$\varepsilon_{yz} = \frac{1+\nu}{E}\sigma_{yz} \tag{1f}$$

where σ_{xx}, σ_{yy}, σ_{zz}, and ε_{xx}, ε_{yy}, ε_{zz}, are the normal stresses and strains, and σ_{xy}, σ_{xz}, σ_{yz}, and ε_{xy}, ε_{xz}, ε_{yz}, are the shear stresses and strains, respectively. Two material parameters are present in Eqs (1), the Young's modulus E and the Poisson's ratio ν; conceptually, there is no difference between the Young's modulus E and the resilient modulus M_R, with the latter name used traditionally in asphalt concrete testing.

The Young's modulus E and the Poisson's ratio ν can be related to another two material constants: the bulk modulus K which links volumetric strains to overall pressure, and

the shear modulus G which links shear (deviatoric) strains to shear (deviatoric) stresses. The relationships between E, ν, K, and G are

$$K = \frac{E}{3(1-2\nu)} \tag{2a}$$

$$G = \frac{E}{2(1+\nu)} \tag{2b}$$

ELASTIC SOLUTION FOR STRESSES AND STRAINS

The elastic solution for stresses and strains, most frequently used as the basis for data interpretation, is the analytic solution given by Hondros (1959). Hondros' solution applies to loading by a uniformly distributed radial pressure p acting over a finite arc and total length of the cylinder (Fig. 2a). In the test interpretation, only the stresses σ_{xx} and σ_{yy} along the centrally located x- and y-axes are used, and they are given by

$$\sigma_{xx}(x,0) = \frac{2P}{\pi aL}\left[\frac{(1-\frac{x^2}{R^2})\sin 2\alpha}{1+2\frac{x^2}{R^2}\cos 2\alpha+\frac{x^4}{R^4}} - \arctan\left(\frac{1-\frac{x^2}{R^2}}{1+\frac{x^2}{R^2}}\tan\alpha\right)\right] \tag{3a}$$

$$\sigma_{yy}(x,0) = -\frac{2P}{\pi aL}\left[\frac{(1-\frac{x^2}{R^2})\sin 2\alpha}{1+2\frac{x^2}{R^2}\cos 2\alpha+\frac{x^4}{R^4}} + \arctan\left(\frac{1-\frac{x^2}{R^2}}{1+\frac{x^2}{R^2}}\tan\alpha\right)\right] \tag{3b}$$

$$\sigma_{xx}(0,y) = \frac{2P}{\pi aL}\left[\frac{(1-\frac{y^2}{R^2})\sin 2\alpha}{1-2\frac{y^2}{R^2}\cos 2\alpha+\frac{y^4}{R^4}} - \arctan\left(\frac{1+\frac{y^2}{R^2}}{1-\frac{y^2}{R^2}}\tan\alpha\right)\right] \tag{3c}$$

$$\sigma_{yy}(0,y) = -\frac{2P}{\pi aL}\left[\frac{(1-\frac{y^2}{R^2})\sin 2\alpha}{1-2\frac{y^2}{R^2}\cos 2\alpha+\frac{y^4}{R^4}} + \arctan\left(\frac{1+\frac{y^2}{R^2}}{1-\frac{y^2}{R^2}}\tan\alpha\right)\right] \tag{3d}$$

where P is the resultant (force) of pressure p, a is the width of the loading strip, L is the length of the cylinder, R is the radius of the cylinder, and 2α is the angle shown in Fig. 2a; compressive stresses are taken as negative. Expressions (3) are independent of Young's modulus E and Poisson's ratio ν, and of whether the cylinder is in plane stress or plane strain condition. Also note that because the central x,y-axes are principal axes for stress, there are no shear stresses along these axes, i.e., $\sigma_{xy}(x,0)= \sigma_{xy}(0,y)= 0$.

Figures 3a and 3b show the distribution of stresses normalized by $\pi RL/P$ for one value of width of the loading strip a/2R=1/8. Along the horizontal x-axis the horizontal stress is tensile, and the vertical stress is compressive. Along the vertical y-axis the vertical stress is compressive whereas the horizontal stress changes from nearly constant tension in the central region to high compression near the loaded boundary.

In contrast to stresses, the strains along the x,y-axes depend on whether the cylinder is in plane stress (short cylinder) or in plane strain (long cylinder) condition. In practice, the cylinders used are short, and the strains are given by

$$\varepsilon_{xx} = \frac{1}{E}(\sigma_{xx} - \nu\sigma_{yy}) \tag{4a}$$

$$\varepsilon_{yy} = \frac{1}{E}(\sigma_{yy} - \nu\sigma_{xx}) \tag{4b}$$

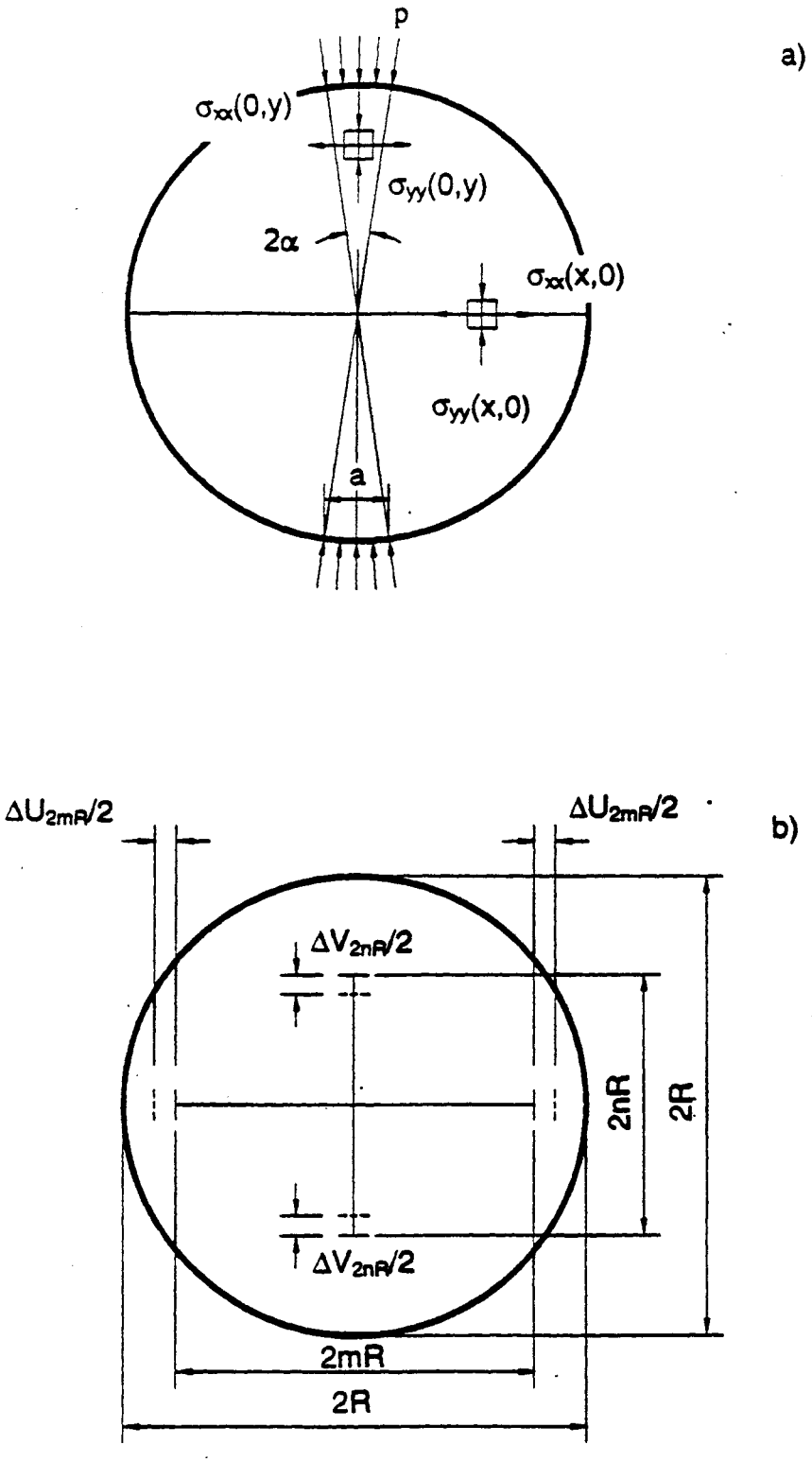

Fig. 2. Diametral compression; a) definitions, b) diametral sectors

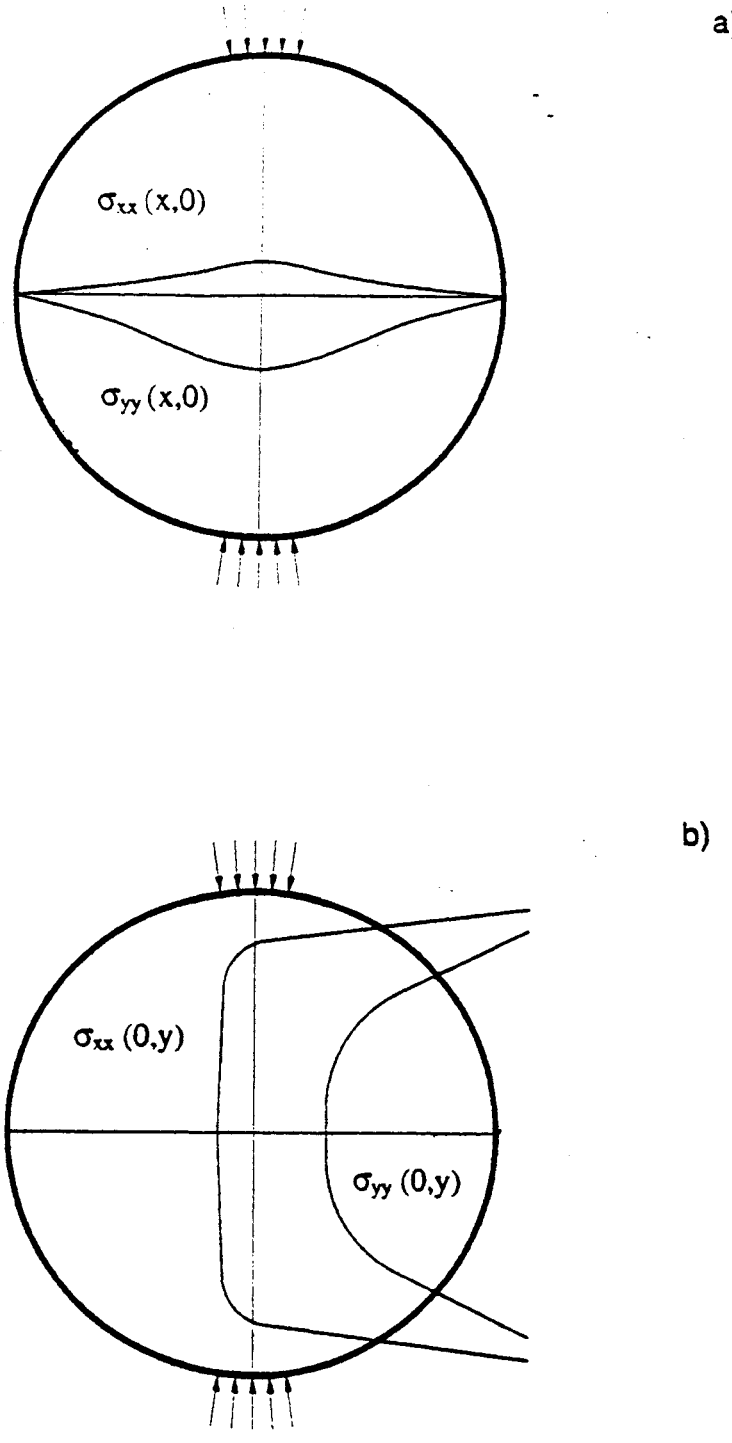

Fig. 3. Stress distributions; a) stresses along horizontal diameter,
b) stresses along vertical diameter

As Eqs (4) imply, the strains depends not only on the stresses but also on the values of the Young's modulus E and Poisson's ratio ν. In the following, not the magnitude of strains in the cylinder but the way the elastic parameters of asphalt concrete can be determined from tests is discussed.

DETERMINATION OF ELASTIC PROPERTIES

The basis for evaluating the elastic parameters E and ν are Eqs (4). In principle, any point along the x,y-axes can be selected for evaluating E and ν if strains ε_{xx} and ε_{yy} corresponding to force P were measured at this point. However, the E and ν evaluated in this way may not be representative for the asphalt concrete as strains vary non-homogeneously throughout the specimen consisting of aggregate, asphalt, and voids, each displaying a different deformability characteristic (stiffness). A more representative approach would be to measure ε_{xx} and ε_{yy} at several points, calculating the corresponding E and ν, and taking an average of their values. An alternative, which is preferable from the experimental view point, is to measure not the local strains but the change in length of two centrally located finite sectors along the x- and y-axes, Fig. 2b. In the following, a sector along the horizontal x-axis of length 2mR, and along the vertical y-axis of length 2nR are considered, where R is the radius of the specimen, and m and n are pure numbers varying between 0 and 1; when m=n=0 the sector is of zero-length (point), and when m=n=1 the sectors become equal to the whole diameter of the cylinder. Then, the change in length of the horizontal sector, ΔU, and of the vertical sector, ΔV, can be expressed as

$$\Delta U = \int_{-mR}^{mR} \varepsilon_{xx}(x,0)dx \tag{5a}$$

$$\Delta V = \int_{-nR}^{nR} \varepsilon_{yy}(0,y)dy \tag{5b}$$

where ΔU and ΔV are positive when the sectors elongate. With the help of Eqs (3) and (4), and the following notation

$$I_1 = \frac{L}{P}\int_{-mR}^{mR} \sigma_{xx}(x,0)dx \tag{6a}$$

$$I_2 = \frac{L}{P}\int_{-mR}^{mR} \sigma_{yy}(x,0)dx \tag{6b}$$

$$I_3 = \frac{L}{P}\int_{-nR}^{nR} \sigma_{xx}(0,y)dy \tag{6c}$$

$$I_4 = \frac{L}{P}\int_{-nR}^{nR} \sigma_{yy}(0,y)dy \tag{6d}$$

we can write relations (5) as

$$\Delta U = \frac{P}{EL}(I_1 - \nu I_2) \tag{7a}$$

$$\Delta V = \frac{P}{EL}(I_4 - \nu I_3) \tag{7b}$$

Rearranging Eqs (7), the elastic parameters can then be determined from

$$E = \frac{I_1 - \nu I_2}{\Delta U}\frac{P}{L} = \frac{I_4 - \nu I_3}{\Delta V}\frac{P}{L} = \frac{I_1 I_3 - I_2 I_4}{I_3 \Delta U - I_2 \Delta V}\frac{P}{L} \tag{8a}$$

$$\nu = \frac{I_4 \Delta U - I_1 \Delta V}{I_3 \Delta U - I_2 \Delta V} \tag{8b}$$

once ΔU and ΔV are measured in the tests. Note that for a given R, a, m, and n, the coefficients I_1, I_2, I_3, and I_4 are constants, as listed in Table 1.

SOLUTION SENSITIVITY

The accuracy of determining the elastic parameters E and ν from Eqs (8) depends on several factors. First of all, the material response may not be purely elastic or, even when elastic, it may be non-linear. Non-linearity in elastic response means that, even though the strains are fully recoverable and time independent, they are non-linear functions of stresses. Stress-dependent non-linearity increases with the increase in the magnitude of stresses, and this may take place in the vicinity of the loading strip where the stresses are high.

Another error may be associated with imperfect contact between the loading strip and the cylindrical surface of the specimen, i.e., different than assumed loading width. Finally, the distribution of the radial pressure along the contact interface may be non-uniform, or accompanied by shear stresses, which is not incorporated in the solution. In fact, the specimen is loaded by a rigid strip inducing displacements rather than uniform pressure.

All these sources of errors point to the contact area of the loading strip, and its vicinity, as the region where the deviations from the theoretical solutions are most likely to occur. It then follows that relying on the measurement of the change in length of the whole vertical diameter of the specimen is questionable, and may lead to inevitable errors in evaluating the elastic parameters of asphalt concrete. In particular, unrealistic values of Poisson's ratio which are often reported, may be an indirect proof of this measurement flaw. Performing displacement measurements over a shorter, centrally located sector of the vertical diameter, on the other hand, may be seen as a viable remedial option, and this is analyzed below in more detail.

Table 1. Values of Constants I

m,n	I_1	I_2	I_3	I_4
a/(2R) = 1/8				
0.25	0.144357	-0.450802	0.155789	-0.488592
0.50	0.233936	-0.780056	0.307445	-1.069463
0.75	0.265925	-0.952670	0.430875	-1.934486
1.00	0.269895	-1.000000	-0.062745	-3.587913
a/(2R) = 1/12				
0.25	0.145731	-0.451662	0.157661	-0.490068
0.50	0.235795	-0.780761	0.313458	-1.075558
0.75	0.267801	-0.952866	0.455791	-1.969691
1.00	0.271760	-1.000000	-0.041736	-4.085948
a/(2R) = 1/100				
0.25	0.146809	-0.452338	0.159133	-0.491231
0.50	0.237250	-0.781312	0.318240	-1.080415
0.75	0.269267	-0.953019	0.477140	-1.999690
1.00	0.273218	-1.000000	-0.004996	-6.750997
a/(2R) = 1/500				
0.25	0.146824	-0.452347	0.159154	-0.491248
0.50	0.237270	-0.781320	0.318307	-1.080480
0.75	0.269288	-0.953021	0.477452	-2.000130
1.00	0.273239	-1.000000	-0.001000	-8.796230

The starting point is the observation that away from the loading strip, the horizontal and vertical stresses along the vertical y-axis are relatively low and nearly constant (Fig. 3). Calculations using different a/2R ratios revealed that the width of the loading area has little effect on these stresses. This is depicted in Figs 4a and 4b, for three a/2R ratios equal 1/8, 1/12, and 1/500. To assess the influence of non-uniform contact pressure, the solutions presented in the previous section were used in conjunction with the principle of superposition. The latter principle allows for constructing the solution as a sum of two or more previous solutions. In the case of applying the load through a rigid block, higher stresses are expected at the corner than in the middle. Figures 5a and 5b show the resulting horizontal and vertical normalized stresses along the x- and y-axis, corresponding to the same total force P and different contact pressure distributions characterized by the ratio p_a/p_0. As in the case of the loaded width, the effect of the non-uniform pressure is hardly noticeable in the central part of the specimen. This result is in agreement with a numerical finite element solution presented by Vinson (1989), who also incorporated the presence of the contact shear stresses.

The results above indicate that measuring the change in length of a vertical central sector shorter than the diameter may indeed alleviate the inaccuracies previously mentioned, and this is supported by the work of Sousa et.al., (1991), and Lytton et.al., (1993). The expressions for calculating E and ν are still Eqs (8) with appropriate value of I_1, I_2, I_3, and I_4. An example where n=0.25 (¼ of vertical diameter), and m=1 (whole horizontal diameter) will be discussed in Chapter 6.

ASTM D4123-82 (1987) and SHRP Protocol P07 (1993)

In ASTM D4123-82 (1987), and SHRP Protocol P07 (1993), the Young's modulus E (resilient modulus M_R), and the Poisson's ratio ν, are calculated from the following expressions

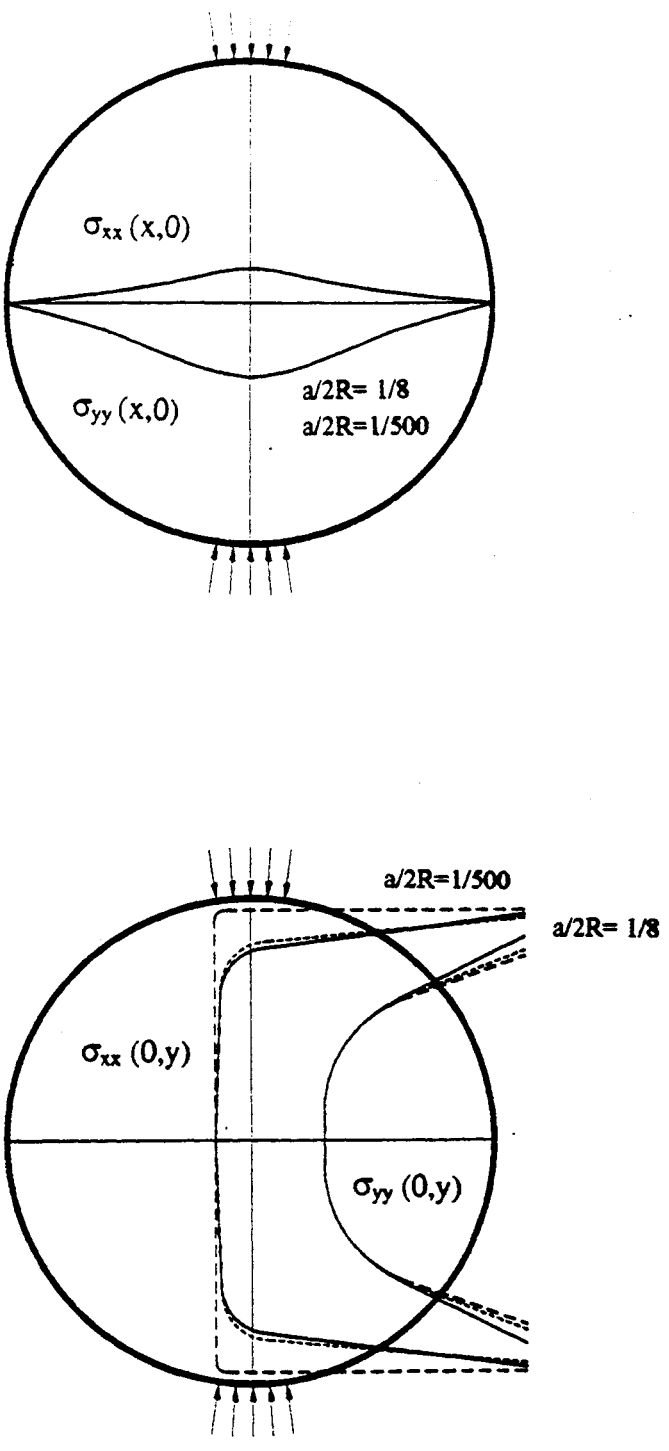

Fig. 4. Influence of the loading width; a) stresses along horizontal diameter
b) stresses along vertical diameter

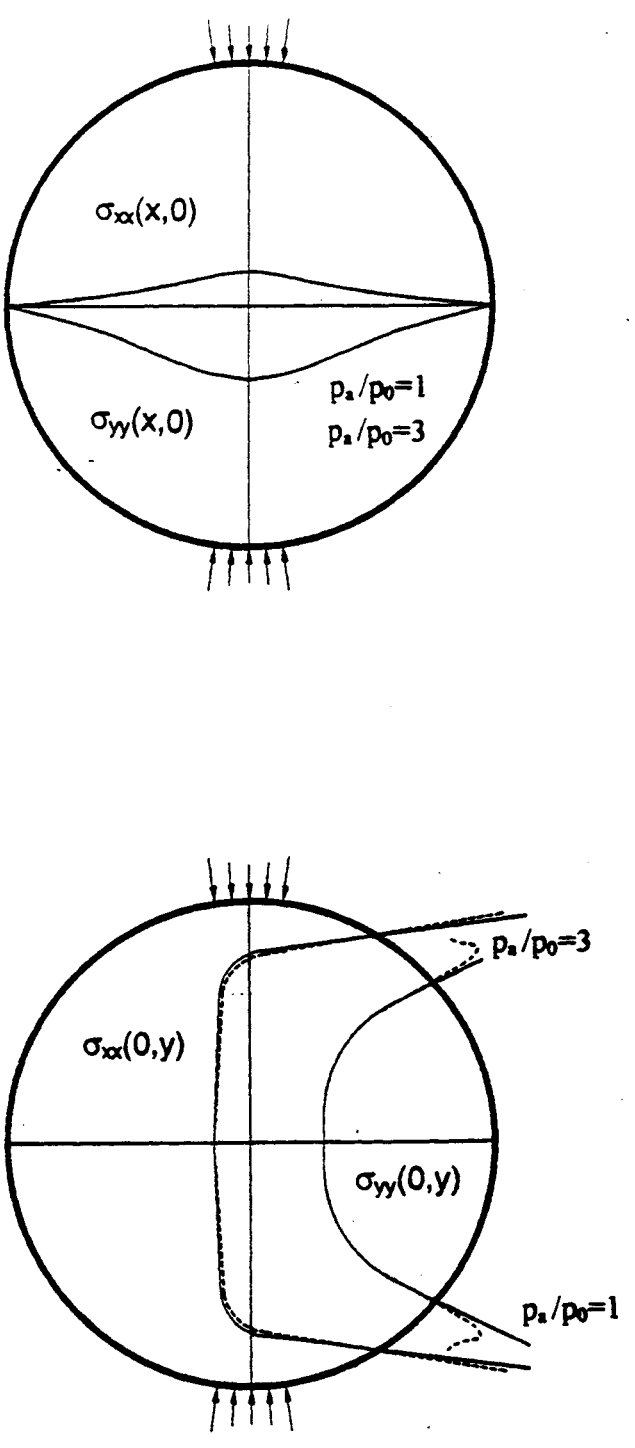

Fig. 5. Influence of pressure distribution; a) stresses along horizontal diameter
b) stresses along vertical diameter

$$E = \frac{0.27 + \nu}{\Delta U} \frac{P}{L} \tag{9a}$$

$$\nu = -3.59 \frac{\Delta U}{\Delta V} - 0.27 \tag{9b}$$

where ΔU and ΔV are the change in length of the whole horizontal and vertical diameter (m=n=1), respectively. Eqs (9) correspond to a/2R=1/8, and Eq (9b) is a simplified form of the equation

$$\nu = \frac{-3.59\Delta U - 0.27\Delta V}{0.063\Delta U + \Delta V} \tag{10}$$

derived from Eq. (8b) when m=n=1, in which the term $0.063\Delta U$ being small is neglected.

It is evident, that neither the ASTM D4123-82 nor the SHRP Protocol P07 take directly into account the possible errors associated with measuring the change of the whole vertical diameter. However, in the ASTM D4123-82 there is reference to assuming rather than calculating Poisson's ratio.

CHAPTER 4
VISCOELASTIC SOLUTION

THE ASSUMPTION OF VISCOELASTICITY

The presence of viscosity in addition to elasticity in a material like asphalt concrete manifests itself as the dependence of strains on the time or rate of loading. This means the stresses and strains are not related by Hooke's law expressed by Eqs (1) which neglects the effect of viscosity altogether. To combine both the elastic and viscous properties of asphalt concrete, a different law must be postulated, and this can be done by following the concepts and mathematical formulation of linear viscoelasticity.

In general, there are two alternative approaches as how the stresses, strains, and the effect of time are interrelated. One approach is based on combining a number of discrete elastic and viscous elements in a parallel or series assemblage, conceptually similar to electronics. Because the response of a viscous element is rate-dependent, the resulting viscoelastic response is described by a stress-strain-time law which is a differential equation with respect to time as opposed to an algebraic equation for an elastic material as is seen in Eqs (1). The response of the material to a specific load history, i.e., constant or varying with time, is obtained by integrating the differential equation.

Examples of this approach are the Maxwell and Kelvin viscoelastic models, each consisting of one elastic and one viscous discrete element. In one-dimensional formulation, each model has two material constants in total, and they can be determined from appropriate tests. However, actual material responses may not match those described by the Maxwell or Kelvin model, and more elements must be added to describe the response adequately. This leads to an increasingly complex stress-strain-time relationship, for adding more viscous elements increases the order of the resulting differential equation. More tests then are required for evaluating material constants, and the stress-strain-time relationship may become unwieldy.

An alternative to these models and the resulting differential equations, is to postulate a relationship between the stress, strain, and time in an integral form. In this formulation,

material functions rather than parameters are introduced, and they are obtained from specified tests. This is advantageous because no assumptions need to be made in advance as to the number of discrete elements which is required in the first approach. The equivalency of both approaches stems from the fact that the operation of integration is, basically, opposite to the operation of differentiation. This means that one form of the relation can be changed to another form by appropriate integration or differentiation.

The choice of material functions that are used in the integral formulation depends on the type of load history of interest. For example, if the load is constant or continuously increasing or decreasing, the most convenient is the creep compliance or relaxation modulus. However, if the load history is periodic, e.g., harmonic or a sum of harmonic loads, it is more convenient to make use of the complex compliance or complex modulus. In the following these concepts are discussed in more detail.

Creep Compliance and Relaxation Modulus

The creep compliance is defined as the quotient of strain and stress in a constant load (creep) test. In one-dimensional formulation, the creep compliance J(t) is given by

$$J(t) = \frac{\varepsilon(t)}{\sigma} \tag{11}$$

where $\varepsilon(t)$ is the strain varying with time, and σ is the constant stress. Geometrically, the constant load test is depicted in Fig. 6a, the strain history in Fig. 6b, and the resulting creep compliance in Fig. 6c. The form of the creep compliance gives some indication as to the contribution of elastic and viscous properties in the overall behavior. For example, the smaller the initial instantaneous part and the greater the time dependent part, the more viscous is the material.

An alternative to creep compliance, but more difficult to determine experimentally, is the relaxation modulus G(t) defined as a quotient of stress to strain when the latter is kept constant

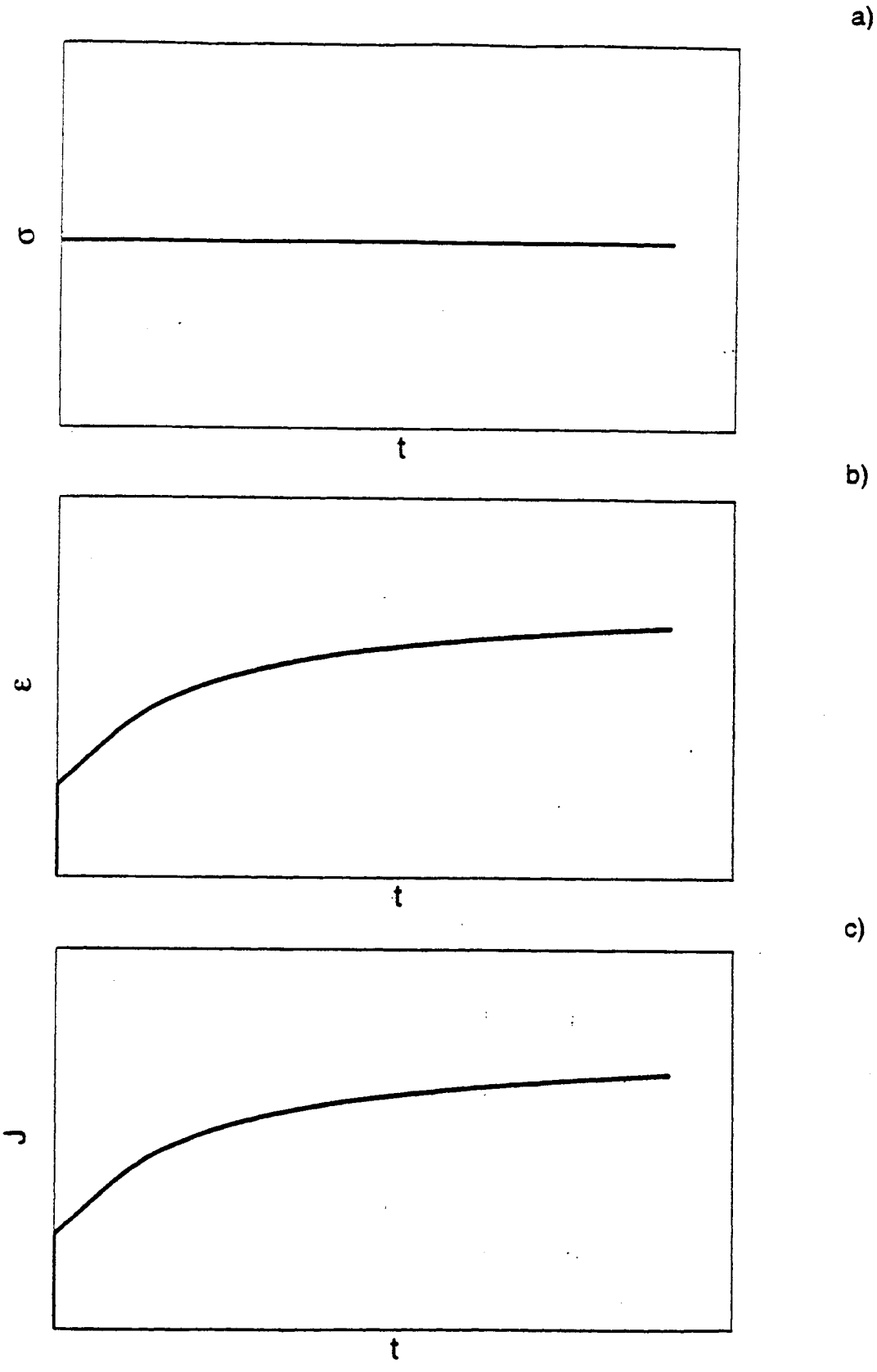

Fig. 6. Stresses and strains in creep test; a) stress history, b) strain history, c) creep compliance

$$G(t) = \frac{\sigma(t)}{\varepsilon} \tag{12}$$

To describe the material behavior under three-dimensional states of stress and strain, it is insufficient to use the one-dimensional creep compliance J(t) or relaxation modulus G(t). When dealing with elastic materials, the three-dimensional response is accounted for by introducing not only the Young's modulus, E, but also the Poisson's ratio, ν. In viscoelasticity, it is more convenient to separate the strains into the volumetric and deviatoric parts, with the latter describing the change in shape. This separation is necessitated because there is significant viscous behavior in shear observed in asphalt concrete, while the volumetric changes tend to be predominantly elastic.

In the general three-dimensional state of strain, the deviatoric and volumetric creep compliances can be defined as

$$J_d(t) = \frac{e_{xx}(t)}{s_{xx}} \tag{13a}$$

$$J_v(t) = \frac{\varepsilon_v(t)}{3\sigma_v} \tag{13b}$$

where

$$e_{xx} = \frac{2\varepsilon_{xx} - \varepsilon_{yy} - \varepsilon_{zz}}{3} \tag{14a}$$

$$s_{xx} = \frac{2\sigma_{xx} - \sigma_{yy} - \sigma_{zz}}{3} \tag{14b}$$

are examples of the deviatoric strains and stresses, and

$$\varepsilon_v = \varepsilon_{xx} + \varepsilon_{yy} + \varepsilon_{zz} \tag{15a}$$

$$\sigma_v = \frac{\sigma_{xx} + \sigma_{yy} + \sigma_{zz}}{3} \tag{15b}$$

are the volumetric strain and stress (pressure), respectively. The response to an arbitrary loading history can then be determined from the following integral equations

$$e_{xx}(t) = \int_{-\infty}^{t} J_d(t-\tau)\frac{ds_{xx}(\tau)}{d\tau}d\tau \tag{16a}$$

$$\varepsilon_v(t) = \int_{-\infty}^{t} J_v(t-\tau)\frac{d\sigma_v(\tau)}{d\tau}d\tau \tag{16b}$$

Complex Compliance and Complex Modulus

In one-dimensional formulation, the harmonic oscillatory stress and strain histories are given by (Fig. 7)

$$\sigma(t) = \sigma_0 \cos\omega t \tag{17a}$$

$$\varepsilon(t) = \varepsilon_0 \cos\omega t \tag{17b}$$

where σ_0 is the stress amplitude, ε_0 is the strain amplitude, and ω is the frequency. The response to these histories is, respectively

$$\varepsilon(t) = \varepsilon_0 \cos(\omega t - \delta) \tag{18a}$$

$$\sigma(t) = \sigma_0 \cos(\omega t - \delta) \tag{18b}$$

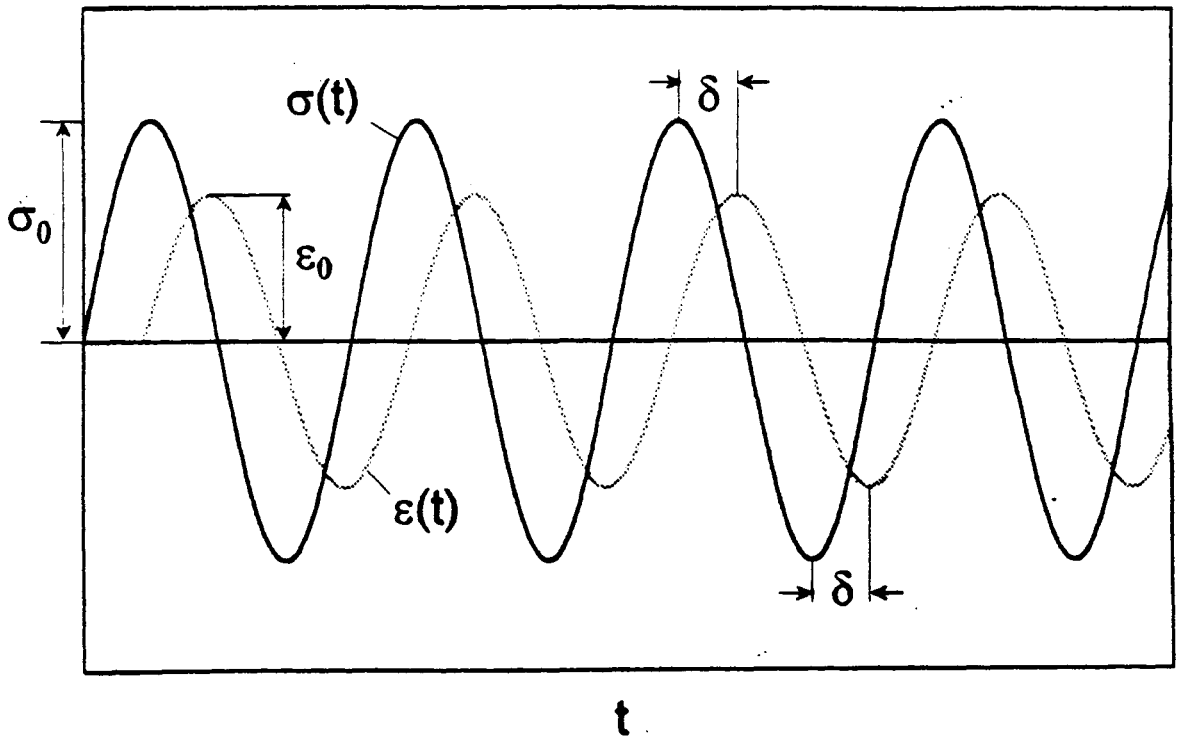

Fig. 7 Stresses and strains in harmonic load history

where δ is the phase angle, whose magnitude depends on the frequency ω.

The complex compliance and complex modulus are defined as

$$J^*(\omega) = J_1(\omega) + iJ_2(\omega) = \frac{\varepsilon_0}{\sigma_0}(\cos\delta - i\sin\delta) \tag{19a}$$

$$G^*(\omega) = G_1(\omega) + iG_2(\omega) = \frac{\sigma_0}{\varepsilon_0}(\cos\delta + i\sin\delta) \tag{19b}$$

where the subscripts $_1$ and $_2$ denote the real and imaginary part, respectively. Between the real and imaginary parts of $J^*(\omega)$ and $G^*(\omega)$, and the phase angle δ, the following relationship applies

$$\tan\delta = \frac{J_2(\omega)}{J_1(\omega)} = \frac{G_2(\omega)}{G_1(\omega)} \tag{20}$$

The quantities defined as

$$|J^*(\omega)| = \sqrt{J_1^{\,2}(\omega) + J_2^{\,2}(\omega)} \tag{21a}$$

$$|G^*(\omega)| = \sqrt{G_1^{\,2}(\omega) + G_2^{\,2}(\omega)} \tag{21b}$$

are called the magnitude of the complex compliance and modulus, respectively, and they are related by

$$|J^*(\omega)||G^*(\omega)| = 1 \tag{22}$$

When considering three-dimensional states of stress and strain, the deviatoric (shear) and volumetric complex compliances, $J^*_d(\omega)$ and $J^*_v(\omega)$, or complex moduli, $G^*_d(\omega)$ and

$G^*_v(\omega)$, are introduced. The amplitudes σ_0 and ε_0 appearing in Eqs (18) then are replaced by the amplitudes of the deviatoric stresses and strains. Likewise, the phase angle δ is replaced by the deviatoric and volumetric phase angles, δ_d and δ_v. For example, the deviatoric complex compliance can be written as

$$J^*_d(\omega) = J_{1d}(\omega) + iJ_{2d}(\omega) = \frac{e_{0xx}}{s_{0xx}}(\cos\delta_d - i\sin\delta_d) \qquad (23)$$

where the subscript $_0$ indicates the amplitude.

The significance of the real and imaginary parts of $J^*_d(\omega)$, $J^*_v(\omega)$, $G^*_d(\omega)$, and $G^*_v(\omega)$, lies in that the real part is related to elastic properties of the material and the imaginary part is related to viscous properties. For a material which is predominantly elastic, the real part is greater than the imaginary part, and the opposite is true for a material which is predominantly viscous. An alternative and perhaps a more direct measure of the ratio of these properties is the phase angle; when this angle is small the elastic properties dominate, and when it is large the viscous properties dominate. Because $|J^*(\omega)|$ and $|G^*(\omega)|$ quantify the overall material deformability without specifying whether it is due to elastic or viscous properties, δ must also be given. It should be remembered, here, that as the numerical values of the compliances, moduli, their real and imaginary parts, and the phase angles are all functions of frequency ω, their spectrum as a function of ω is required to assess the elastic and viscous properties fully. However, the range of frequencies should also encompass those simulating the actual loading conditions, i.e., traffic. It should be mentioned at this point that it is possible to derive relationships between the complex compliance $J^*(\omega)$ and the creep compliance J(t), and between the complex modulus $G^*(\omega)$ and the relaxation modulus G(t).

VISCOELASTIC SOLUTION FOR STRESSES AND STRAINS

One of the most powerful methods of solving viscoelastic problems is based on the so-called elastic-viscoelastic correspondence principle. The correspondence principle dwells on the similarity between the elastic stress-strain relationship and the viscoleastic stress-strain-time relationship if the latter is transformed from the time domain to another domain by means of the Laplace or Fourier integral transform. This similarity implies that to obtain the viscoelastic solution, the elastic solution can first be constructed and then transformed, with the elastic constants replaced by appropriate transforms of the viscoelastic compliances or moduli. The actual viscoelastic solution is obtained by performing an inverse transform.

The Laplace transform is useful when a non-periodic load history is applied to the material, e.g., constant or continuously increasing or decreasing load. The replacement rules for the parameters then are

$$E \rightarrow \frac{1}{\frac{2}{3}s\bar{J}_d(s) + \frac{1}{3}s\bar{J}_v(s)} \tag{24a}$$

$$\nu \rightarrow \frac{\bar{J}_d(s) - \bar{J}_v(s)}{2\bar{J}_d(s) + \bar{J}_v(s)} \tag{24b}$$

where the bar indicates the transformed quantity, and s is the Laplace variable replacing the time t. The Fourier transform, on the other hand, is convenient whenever the load is periodic or a sum of periodic loads, e.g., the pulse/rest load history and the haversine load history. Then,

$$E \rightarrow \frac{1}{\frac{2}{3}J^*_d(\omega) + \frac{1}{3}J^*_v(\omega)} \tag{25a}$$

$$\nu \rightarrow \frac{J^*_d(\omega) - J^*_v(\omega)}{2J^*_d(\omega) + J^*_v(\omega)} \tag{25b}$$

The basis for deriving the viscoelastic solution of the diametral compression test by means of the correspondence principle is the elastic solution presented in Chapter 3. In this solution, the stresses along the central vertical and horizontal axes are given by Eqs (1) which do not contain material constants E and ν. This means that applying the Laplace or Fourier transforms and their inverse to these expressions will not change them. In other words, the stresses in a diametrically compressed cylinder are the same regardless as whether the material is elastic or viscoelastic.

This is not the case with strains whose magnitude and variation in time can be determined for a given load history by subjecting Eqs (15) to Laplace or Fourier transform, replacing E and ν by appropriate viscoelastic functions according to Eqs (24) or (25), and performing the inverse transforms. Likewise in Chapter 3, rather than analyzing strains, the inverse problem is considered below, namely, how to determine the viscoelastic properties of asphalt concrete, from measurements of the change in length of the diametral sectors of the cylinders.

DETERMINATION OF VISCOELASTIC PROPERTIES

In general, any load history applied to the cylinder can be used to determine the viscoelastic properties of asphalt concrete. In the following, however, only three specific histories will be discussed: a) the constant load history (creep test) followed by a rest period, b) the haversine load history, and c) the pulse/rest load history.

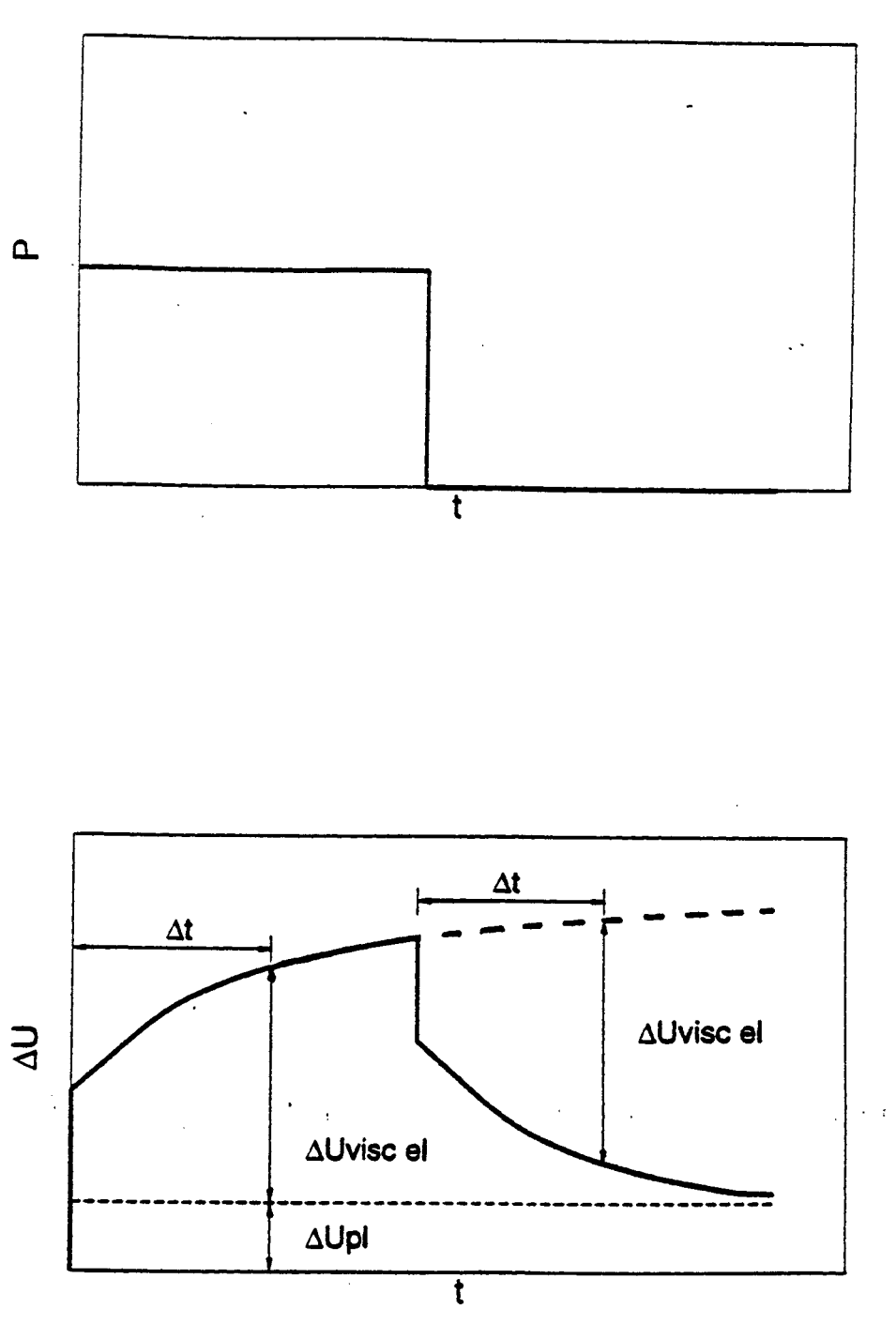

Fig. 8. Constant load/rest test; a) load history, b) deformation history

Constant Load (Creep) History

For the constant load history followed by a rest period (Fig. 8)

$$P(t) = P_0 = \text{const} \qquad \text{creep} \tag{26a}$$

$$P(t) = 0 \qquad \text{rest} \tag{26b}$$

and with the help of Eqs (4), (5), and the Laplace transform, and Eqs (12), the expressions for the deviatoric and volumetric creep compliances can be written as

$$J_d(t) = \frac{K_4\Delta U - K_2\Delta V}{K_1K_4 - K_2K_3}\frac{L}{P_0} \tag{27a}$$

$$J_v(t) = \frac{K_1\Delta V - K_3\Delta U}{K_1K_4 - K_2K_3}\frac{L}{P_0} \tag{27b}$$

where ΔU and ΔV are measured during creep, and K_1, K_2, K_3, and K_4 are constants related to constants I_1, I_2, I_3, and I_4 by (see Table 2)

$$K_1 = \frac{1}{3}(2I_1 - I_2) \tag{28a}$$

$$K_2 = \frac{1}{3}(I_1 + I_2) \tag{28b}$$

$$K_3 = \frac{1}{3}(2I_4 - I_3) \tag{28c}$$

$$K_4 = \frac{1}{3}(I_4 + I_3) \tag{28d}$$

If the tested material displays plastic properties in addition to viscoelastic properties, which often is the case with asphalt concrete (Drescher et.al., 1993), the contribution of

Table 2. Values of constants K

m,n	K_1	K_2	K_3	K_4
a/2R=1/8				
0.25	0.246	-0.102	-0.377	-0.111
0.50	0.416	-0.182	-0.815	-0.254
0.75	0.494	-0.229	-1.433	-0.501
1.00	0.513	-0.243	-2.371	-1.217
a/2R=1/12				
0.25	0.247	-0.102	-0.379	-0.111
0.50	0.417	-0.181	-0.821	-0.254
0.75	0.496	-0.228	-1.465	-0.504
1.00	0.514	-0.243	-2.710	-1.376
a/2R=1/100				
0.25	0.248	-0.102	-0.380	-0.111
0.50	0.418	-0.181	-0.826	-0.254
0.75	0.497	-0.228	-1.492	-0.506
1.00	0.515	-0.242	-4.499	-2.252
a/2R=1/500				
0.25	0.248	-0.102	-0.380	-0.111
0.50	0.418	-0.181	-0.826	-0.254
0.75	0.497	-0.228	-1.492	-0.507
1.00	0.515	-0.242	-5.864	-2.932

plastic deformation must be eliminated from the measured ΔU and ΔV. This can be done by extending the creep curve over the rest period, and determining ΔU and ΔV as the difference between the extended creep curve and the recovery curve (Fig. 8).

Haversine Load History

The load history which allows for determining the complex compliance and its real and imaginary parts directly is the harmonic load history given by Eq. (17a) with force P substituted for stress σ. Since the cos-function changes signs, realization of harmonic load would require subjecting the specimen to periodic tension-compression. This is difficult to perform, and the common practice is to restrict the loading to compression by superimposing harmonic load and constant load histories which results in a haversine load history. In practice, the following history is applied

$$P(t) = P_1 - P_0 \cos\omega t \tag{29}$$

where P_1 is a sum of constant load P_0 and a small load ΔP applied to maintain the loading strips and the specimen in contact. The presence of load P_1 causes change in ΔU and ΔV due to creep of asphalt concrete, and this contribution must be separated for proper evaluation of the amplitudes and phase angles. This is demonstrated in Fig. 9 which illustrates the variation of ΔU in a haversine load test. The amplitude of the harmonic part ΔU_0 is indicated in this figure. Also, two apparent (false) phase angles are denoted as δ^l (loading) and δ^u (unloading); the true phase angle is the mean of the two. This applies equally to amplitudes and phase angle of ΔV. It should be stressed at this point, that by separating the creep contribution the possible plasticity-related effect also is eliminated.

Using Eqs (4), (5), (14), and (25), the expressions for the real and imaginary parts of the deviatoric and volumetric complex compliances become

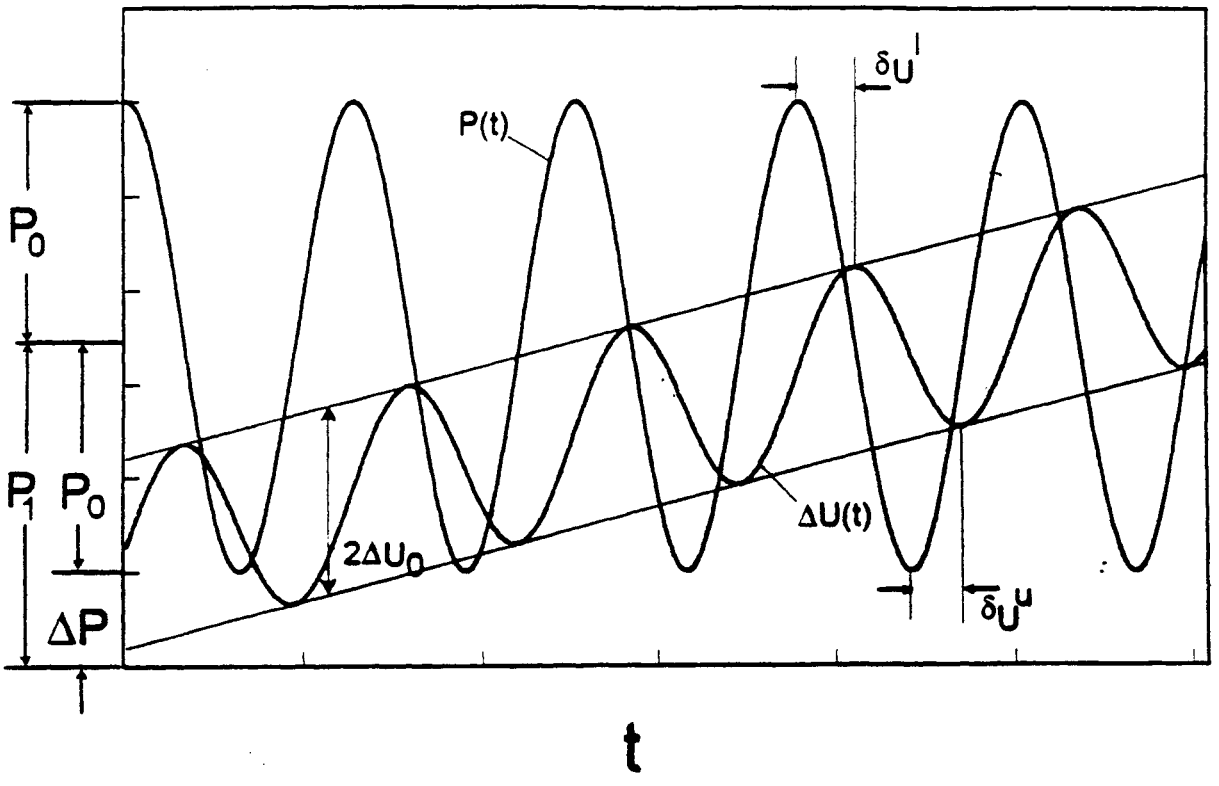

Fig. 9. Haversine load test

$$J_{d1}(\omega)=\frac{K_4\Delta U_0\cos\delta_U+K_2\Delta V_0\cos\delta_V}{K_1K_4-K_2K_3}\frac{L}{P_0}$$

(30a)

$$J_{d2}(\omega)=-\frac{K_4\Delta U_0\sin\delta_U+K_2\Delta V_0\sin\delta_V}{K_1K_4-K_2K_3}\frac{L}{P_0} \tag{30b}$$

$$J_{v1}(\omega)=\frac{K_1\Delta V_0\cos\delta_V+K_3\Delta U_0\cos\delta_U}{K_1K_4-K_2K_3}\frac{L}{P_0} \tag{30c}$$

$$J_{v2}(\omega)=-\frac{K_1\Delta V_0\sin\delta_v+K_3\Delta U_0\sin\delta_U}{K_1K_4-K_2K_3}\frac{L}{P_0} \tag{30d}$$

where the subscript $_0$ signifies the amplitude, and δ_U and δ_V are the phase angles of the measured in tests ΔU and ΔV.

Pulse/rest Load History

The pulse/rest load history is recommended for resilient moduli determination in ASTM D4123-82 and SHRP Protocol P07 procedures. It consists of a sequence with period T of a haversine load pulse of duration 2d followed by a rest period of duration T-2d (Fig. 1). This can be expressed as

$$P(t)=P_1-P_0\cos\frac{\pi}{d}t \qquad \text{pulse} \tag{31a}$$

$$P(t)=0 \qquad \text{rest} \tag{31b}$$

Because the pulse/rest load history is neither a constant load nor pure haversine

history, it cannot be used directly for determining the viscoelastic properties of asphalt concrete. Theoretically, the pulse/rest history could be approximated by a Fourier series of harmonic load histories. The overall response of the material than can be regarded as a sum of responses to individual harmonic loadings, each with a corresponding complex compliance. Satisfactory approximation of the pulse/rest history, however, requires using a high number of terms of the Fourier series and, hence, a high number of complex compliances must be determined from the experimental data. The resulting regression process becomes extremely tedious, time consuming, and may be highly inaccurate. For these reasons, using the pulse/rest load history for determining the viscoelastic properties of asphalt concrete is impractical if not impossible.

SOLUTION SENSITIVITY

Since the basis for the viscoelastic solution is the elastic solution discussed previously, all the comments regarding the sensitivity of the elastic solution to deviations from material linearity and imperfect application of load presented in Chapter 3 equally apply to the the viscoelastic solution. Specifically, errors may occur in determining the viscoelastic properties of asphalt concrete if the measurements of the change in length in the vertical direction are taken over the whole diameter, i.e., when n=1. Much more reliable results are expected from measuring the change of length of a centrally located vertical sector shorter than the diameter, e.g., ¼ of diameter when n=0.25.

CHAPTER 5
DIAMETRAL COMPRESSION TESTS

This chapter describes a series of diametral compression tests conducted to illustrate the theoretical findings presented in Chapters 3 and 4. More specifically, the objective of the tests was to obtain data that can be used to determine the viscoelastic properties characterizing asphalt concrete response to single and repeated load histories. The tests were conducted in two groups. In Group 1, the specimens fabricated from two mixtures were subjected to various load histories at one temperature. In Group 2, the specimens fabricated from eight different mixtures typifying Mn/ROAD materials, were tested at two specific load histories but three different temperatures.

MATERIALS

Aggregate

The aggregate for Group 1 specimens was obtained from two sources: 1) the 9.5 mm (3/8 in.) through 19 mm (3/4 in.) fractions of 100% crushed granite, were obtained from Meridian Inc., Granite Falls, Minnesota, quarry, and 2) the 4.75 mm (No.4) and below fractions of partially crushed river gravel, were obtained from the Commercial Asphalt, Inc., Lakeland, Minnesota, quarry. Figure 10 shows the aggregate gradation, and Table 3 gives the physical properties.

In Group 2 specimens a dense-graded aggregate was used. It consisted of 10% crushed granite from Meridian Inc., St.Cloud, Minnesota, and 90% of partially crushed river gravel from the Crow River gravel pit in Buffalo, Minnesota (see Stroup-Gardiner and Newcomb, 1996).

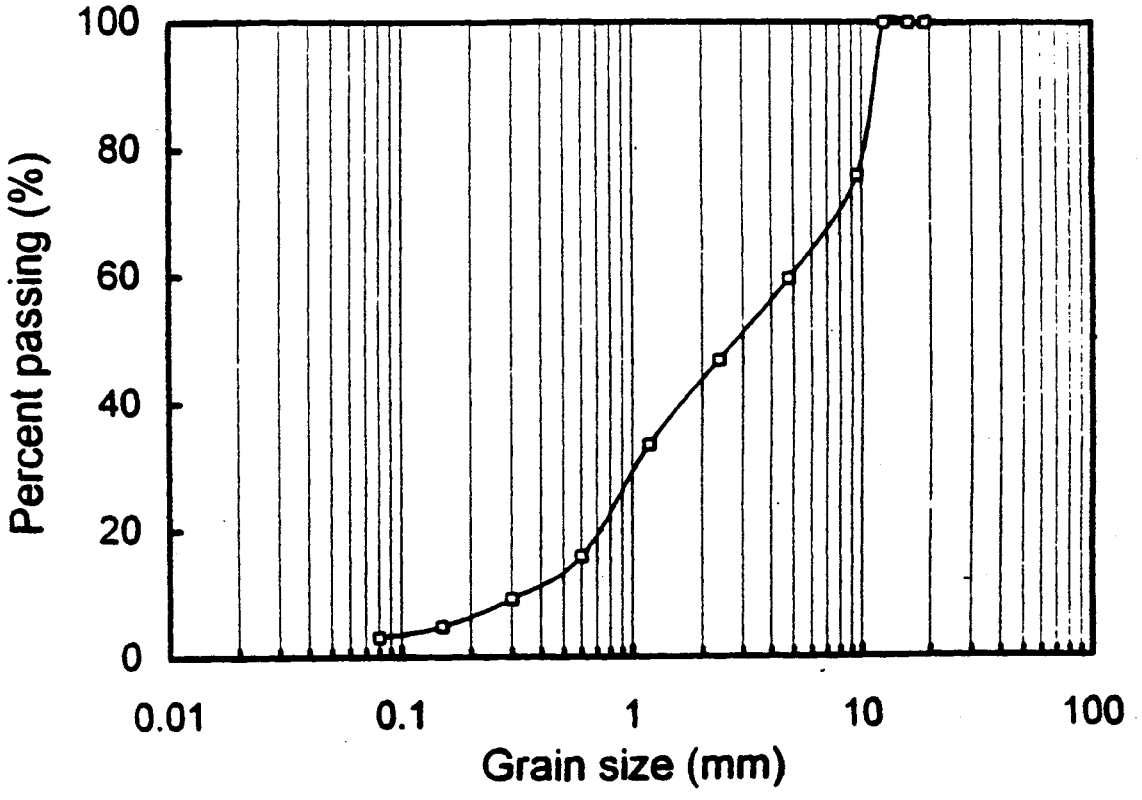

Fig. 10. Aggregate gradation - Group 1

Table 3. Physical Properties of Aggregates

Aggregate	Bulk Specific Gravity	Bulk Specific Gravity, SSD	Absorption, %
River gravel	2.582	2.650	2.6
Crushed granite	2.648	2.660	0.4

Table 4. Properties of Asphalt Cements

Properties	AASHTO Method	Asphalt Grade AC20	120/150
Penetration @ 25°C, 0.1mm, 5 sec	T 49	83	133
Absolute viscosity @ 60°C, poises	T 202	1797	807
Kinematic viscosity @ 135°C, cs	T 201	377	265
Flash point, °C	T 48	282	134
Ductility, 25°C, 5cm/min, cm	T 51	+100	+100
Solubility, %	T 44	99.9	99.9
Specific Gravity	T 228	1.04	1.03

Asphalt Cement

Two grades of asphalt cement, an 120/150 penetration grade asphalt, and an AC20 viscosity grade asphalt came from the Koch Refinery Co., Inver Grove Heights, Minnesota. Some of the physical properties of the asphalt cements are shown in Table 4.

MIXTURES AND SPECIMENS

All mixtures within a group were prepared with the same aggregate. However, different asphalt binders were used, and different compaction methods or compaction efforts were utilized. This is described separately for specimens of Group 1 and Group 2. The diameter of all specimens was 102 mm (4 in.), and their height was approximately 63.5 mm (2.5 in.).

Group 1

Two different types of mixtures were made. Mixture A was made with the AC20 viscosity grade asphalt, the harder binder, and mixture B was made with the 120/150 penetration grade asphalt, the softer binder. The same aggregate gradation, asphalt content, and compaction effort were used for both mixtures. The optimum asphalt content was determined as 4.58% by total weight of the mixture for both groups using the conventional Marshall mixture design procedure.The specimens were prepared using a Marshall compactor and 50 blows per side of the specimen. Nine specimens were prepared from each mixture. The physical properties of the mixtures are listed in Table 5.

Table 5. Properties of Mixtures - Group 1

	Mixture A	Mixture B
Theoretical maximum specific gravity	2.552	2.503
Air void content (%)	6.69	4.64
Bulk Specific Gravity	2.379	2.384

Table 6. Properties of Mixtures - Group 2

Mix Design Method	Optimum Asphalt Cement Content	VMA %	VFA %
35 Blow Marshall	6.4	17.4	78.5
50 Blow Marshall	6.1	16.8	74.4
75 Blow Marshall	5.9	16.5	75.0
SHRP Gyratory Level 1	5.6	15.5	74.0

Table 7. Group 1 Replicates

	Replicate	
	Mixture A	Mixture B
Indirect tensile strength test	1	1
Resilient modulus test	6	6
Constant load test	6	6
Haversine load test	6	6

Group 2

Four asphalt contents were selected for each of the two asphalt grades (AC20 and 120/150 penetration grade), depending upon the compaction level used in the mix design process (eight in total mixtures). Marshall mix designs were completed by Mn/DOT using 35-, 50-, and 75-blow per face compactive efforts. Additionally, a fourth mix design was performed by the Asphalt Institute using the Strategic Highway Research Program's gyratory compactor. For an air void level of four percent, the optimum asphalt content decreased with increasing compaction as shown in Table 6.

EQUIPMENT, INSTRUMENTATION, AND DATA ACQUISITION

The tests were conducted using an MTS 810 universal servo-controlled load system. The system allows for applying load up to 100 kN (22 kips), and can be used for compression, tension, fatigue, fracture mechanics testing and other standard tests. The diametral compression was induced through concave, steel loading strips of width 1/8 of the specimen diameter and a radius of 51 mm (2 in.).

The measurements during the test included the load applied to the specimen and the change in length (deformation) of a horizontal and a vertical sector of the specimen diameter. The ASTM D4123-82 and SHRP P07 Protocol procedures mandate measuring the change in length across the whole horizontal diameter and the change in length across the whole vertical diameter. The sensitivity analysis presented in Chapter 3, however, suggests that measuring the change in length of a vertical sector located away from the regions next to the loading strips, should provide more reliable results. To verify this conjuncture, the measurements of the change in length were performed for the whole vertical diameter, and for a centrally located vertical sector of ¼ diameter length. In the horizontal direction, the change in length was measured for the whole diameter.

The change in length of the whole horizontal diameter was measured using an MTS 632.94-20 extensometer with lateral attachment kit. The change in length of the whole vertical diameter was measured with the built-in LVDT inside the actuator, and of the ¼ diameter

central sector by means of an in-house modified MTS 632.06 displacement gage. The travel range of both the extensometer and the displacement gage is ±4.00 mm (±0.160 in.).

The MTS 632.06 displacement gage comes with only one arm, and is originally designed to be placed against the specimen surface or an active component in the force train. In order to measure the relative displacement between two points along the central sector of the vertical diameter, the gage was modified to a clip-on gage, Fig. 11. The base length of the modified gage is determined by the two spacers, which are glued to the surface of the specimen by a small amount of epoxy resin. A fixture was built to place the spacers 25.4 mm (1 in.) or 50.8 mm (2 in.) apart onto the specimen surface. This setup can be quickly attached or detached, and produces no interference with the extensometer used for measuring the horizontal displacements.

Data acquisition was achieved using the Data Translation DT2809 single board analog I/O system. The board was plugged into one of the expansion slots in the IBM compatible computer, and programmed to perform analog to digital (A/D) conversion, digital to analog (D/A) conversion, and digital input and digital output transfers. When operating under the Dynamic Memory Access (DMA) mode, the A/D conversion rate can be up to 16 kHz.

DATA ACQUSITION SOFTWARE

The MTS-810 system allows for conducting many kinds of tests, both static and dynamic, and the electronic instruments are capable of measuring the load and displacements at very high resolution and speed. However, a properly designed software is required to control the testing machine and collect data during the test.

The data acquisition software was developed to achieve the following objectives: 1) to create any waveform, 2) to make necessary adjustments to protect the equipment without interrupting the test when the specified load or data collection frequency exceeds the equipment's capacity, 3) to be able to conduct a sequence of tests on the same specimen without user participation, 4) to have both digital and real time graphic displays to allow the user to evaluate the test results directly and to take proper action in case of machine

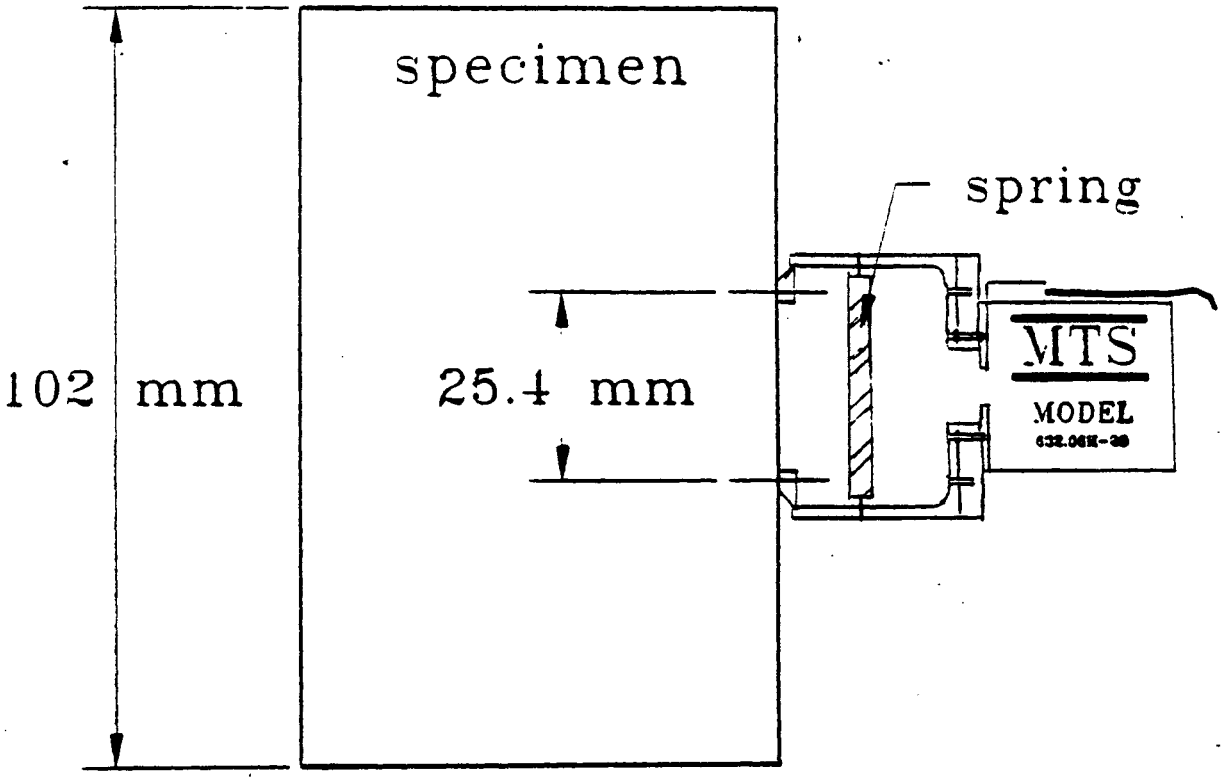

Fig. 11. Clip-on displacement gage

malfunction, and 5) to generate formatted data files that facilitate both spreadsheet and custom designed software processing.

The data acquisition software was coded in Quick Basic™ and requires a VGA monitor for real time graphic display. Communication between the computer and the MicroProfiler was made through the RS232 serial interface at a baud rate of 9600. Both load controlled and displacement controlled test can be conducted, and any type of load waveform composed of the three basic segments (ramp, sine, and hold time) can be generated. The software is versatile enough to run a variety of tests.

The software contains four modules: function generator, data acquisition option, test execution, and quit. The function generator module allows the user to define the desired wave-form. The data acquisition option module lets the user specify the cartridge ranges of the load channel and the displacement channels, so that proper calibrations can be made. It also allows the user to specify the data collection frequency in terms of number of data points per cycle, and the desired data file name. The test execution module downloads the user input wave-form segments to the MicroProfiler, activates the hydraulic system, executes the test, collects data at specified frequencies, creates the data files, and turns off the hydraulic system after finishing the test. The quit module terminates the program.

GROUP 1 TESTS

The tests consisted of the indirect tensile strength test, resilient modulus test, haversine load test, and constant load (creep) test. All tests were conducted at one temperature of 25°C (77°F). Except the indirect tensile strength test, where the specimens are tested up to failure, all other tests were regarded as non-destructive, and the same specimen was subjected to various load histories. Table 7 summarizes the number of test replicates.

Indirect Tensile Strength Tests

The indirect tensile strength tests were conducted as displacement controlled, with the specimen compressed at a rate of 0.85 mm/sec (2 in./min) which resulted in failure in about one minute. The purpose of this test was to determine the maximum load needed to break the specimen. This load was used as a reference to determine the load level to be used in all other tests. One specimen from each mixture was used for this test. The measurements recorded during the test included the load, P, and the change in length of the whole vertical diameter. The maximum load for the A-mix specimen was 12,500 N (2,810 lbf), and for the B-mix specimen it was 5,600 N (1,259 lbf).

Resilient Modulus Tests (Pulse/rest load)

In the resilient modulus tests the specimens were subjected to pulse/rest load at three frequencies specified in the ASTM D4123-82 as 0.33, 0.5, and 1 Hz, with the duration of the load pulse 0.1 sec. The tests were conducted at pulse load P=1500 N (337 lbf), and rest load P=50 N (11 lbf) to prevent separation of the loading strip from the specimen; the pulse load selected is well below the failure load yet adequate for high resolution measurements. Each specimen was preconditioned to 30 load cycles at 0.33 Hz frequency and to 100 load cycles at 1 Hz frequency.

The measurements recorded during the test included the time t, load P, the change in length over the whole horizontal diameter, the change in length over the whole vertical diameter, and the change in length over the central ¼ of the vertical diameter. Figures 12 and 13 show examples of the results obtained.

Haversine Load Tests

The haversine load tests were conducted at maximum load P=550 N (124 lbf) and minimum load P=50 N (11 lbf); this corresponds to harmonic part of load of amplitude P_0=250 N (56 lbf). The maximum load was lower than that used in the pulse/rest tests to

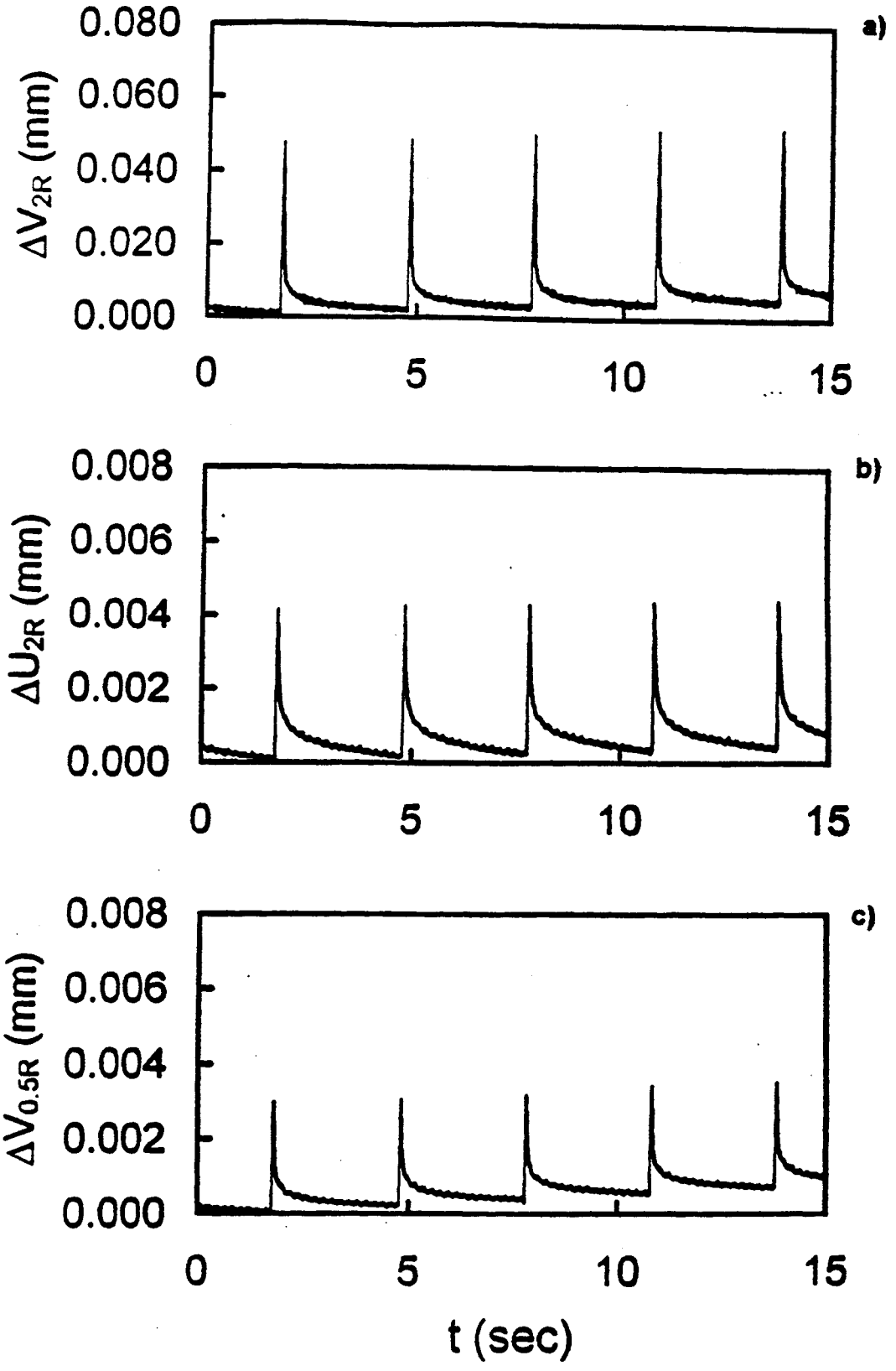

Fig. 12. Pulse/rest test - A mixture; a) change in length of vertical diameter, b) change in length of horizontal diameter, c) change in length of ¼ vertical diameter

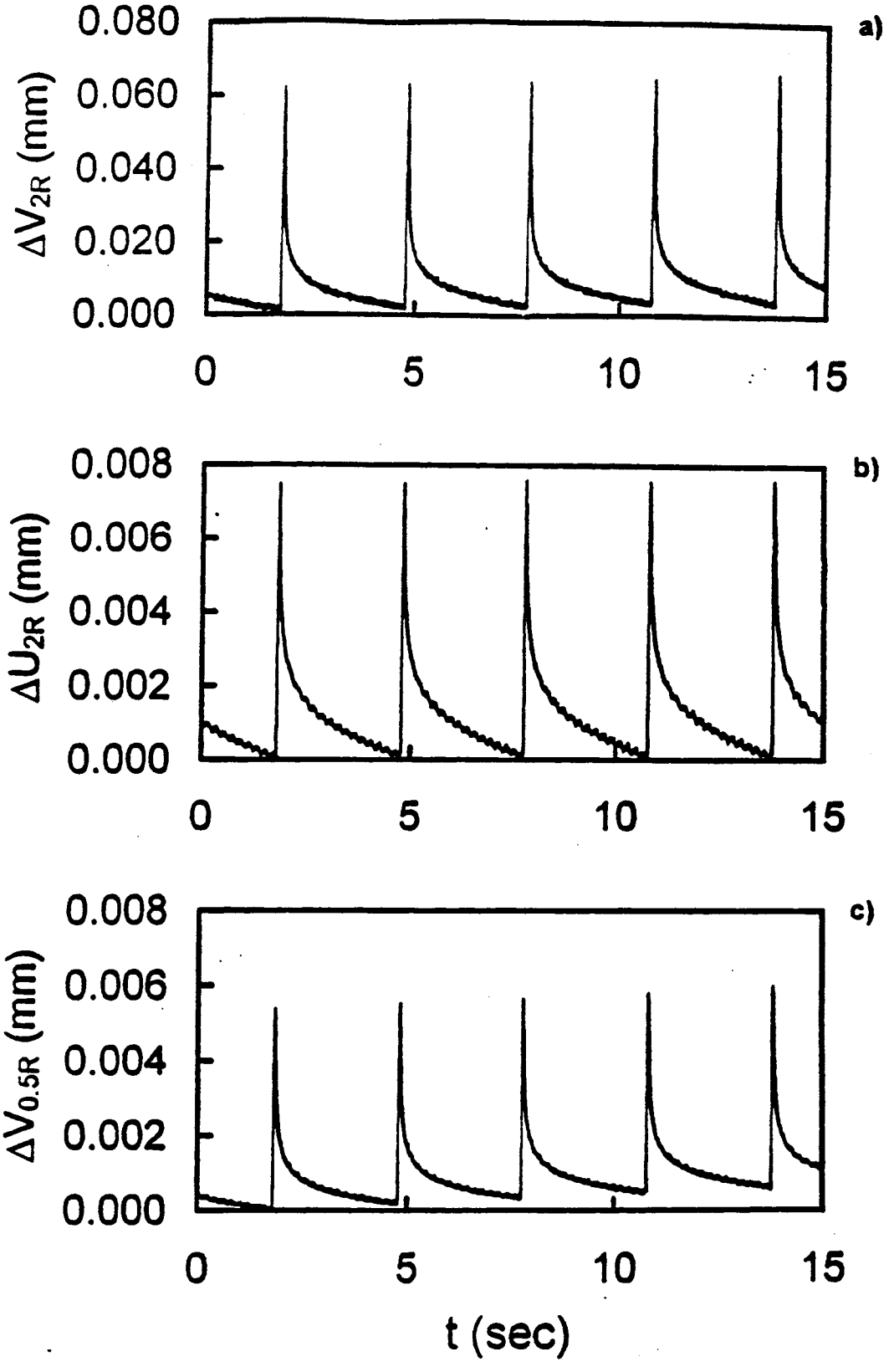

Fig. 13. Pulse/rest test - B mixture; a) change in length of vertical diameter, b) change in length of horizontal diameter, c) change in length of ¼ vertical diameter

avoid excessive deformation resulting from subjecting each specimen to several load frequencies; the small minimum load was used to prevent loading strips/specimen separation. To investigate material response over a wide range of frequencies, each specimen was subjected to the following load frequencies: 0.03, 0.1, 1, 5, 10, 20, 30, 40, 50, 60, 70, and 80 Hz. The measurements were the same as in the resilient modulus tests.

Typical test results are depicted in Figs. 14 and 15, when the response of the material could be regarded as steady; this required from 10 load cycles for the low frequencies to 300 load cycles for the higher frequencies. The dashed lines in Figs. 14 and 15 represent smoothed response obtained with the help of a data regression program.

Constant Load (Creep) Tests

The creep tests were conducted by applying a constant load P=550 N (124 lbf) at the end of haversine tests for the period of 10 min, which was followed by a 10 min rest period with a small load P=50 N (11 lbf). Again, the small rest period load was applied to prevent separation of the loading strips from the specimens. Six specimens of each mixture were tested. The measurements recorded during the creep test were the same as in the resilient modulus and haversine load tests.

Figures 16 and 17 illustrate the measured variation of ΔU and ΔV with time t.

GROUP 2 TESTS

In this group, the haversine load tests, and the resilient modulus tests were conducted at three temperatures: -18°C (0°F), 1°C (33°F), and 25°C (77°F). Each specimen was subjected to one load history and one temperature only. Table 8 shows the number of test replicates.

Haversine Load Tests

The tests were conducted at two frequencies, 0.1 Hz and 1 Hz. The loads varied between the maximum load of 800 N (180 lbf) at T=-18°C (0°F), 500 N (112 lbf) at T=1°C

(33°F), and 200 N (45 lbf) at T=25°C (77°F), and the same at all temperatures minimum load of 50 N (11 lbf). The measurements included the load P, the change in length of the whole horizontal diameter, and of the central, ¼ diameter vertical sector.

Resilient Modulus Tests (Pulse/rest load)

These tests were carried out at one frequency of 1 Hz, with the 0.1 sec duration of the pulse and 0.9 sec rest period. The loads and the measurements were the same as in the haversine load tests.

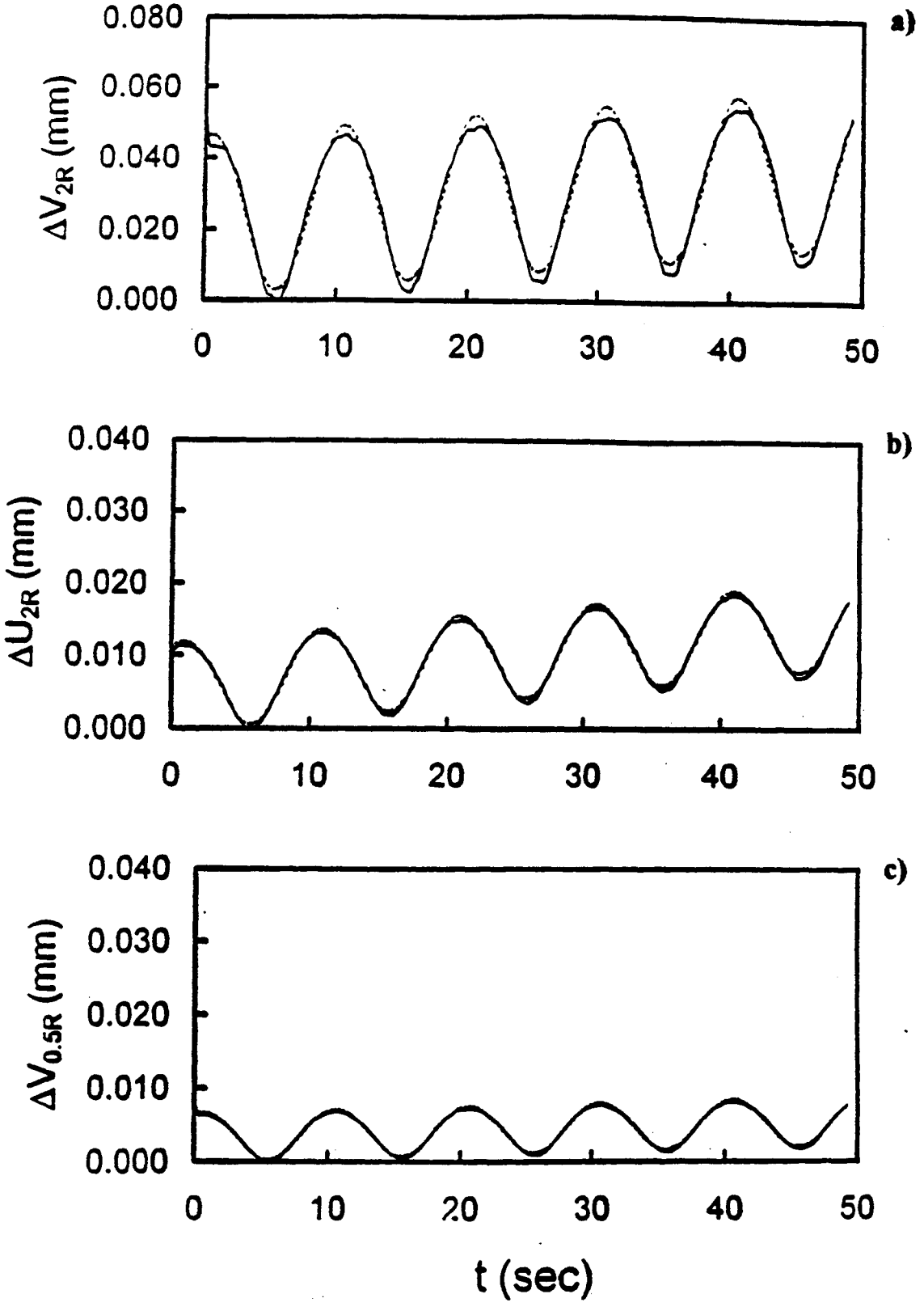

Fig. 14. Haversine test - B mixture, ω=0.1 Hz; a) change in length of vertical diameter, b) change in length of horizontal diameter, c) change in length of ¼ vertical diameter

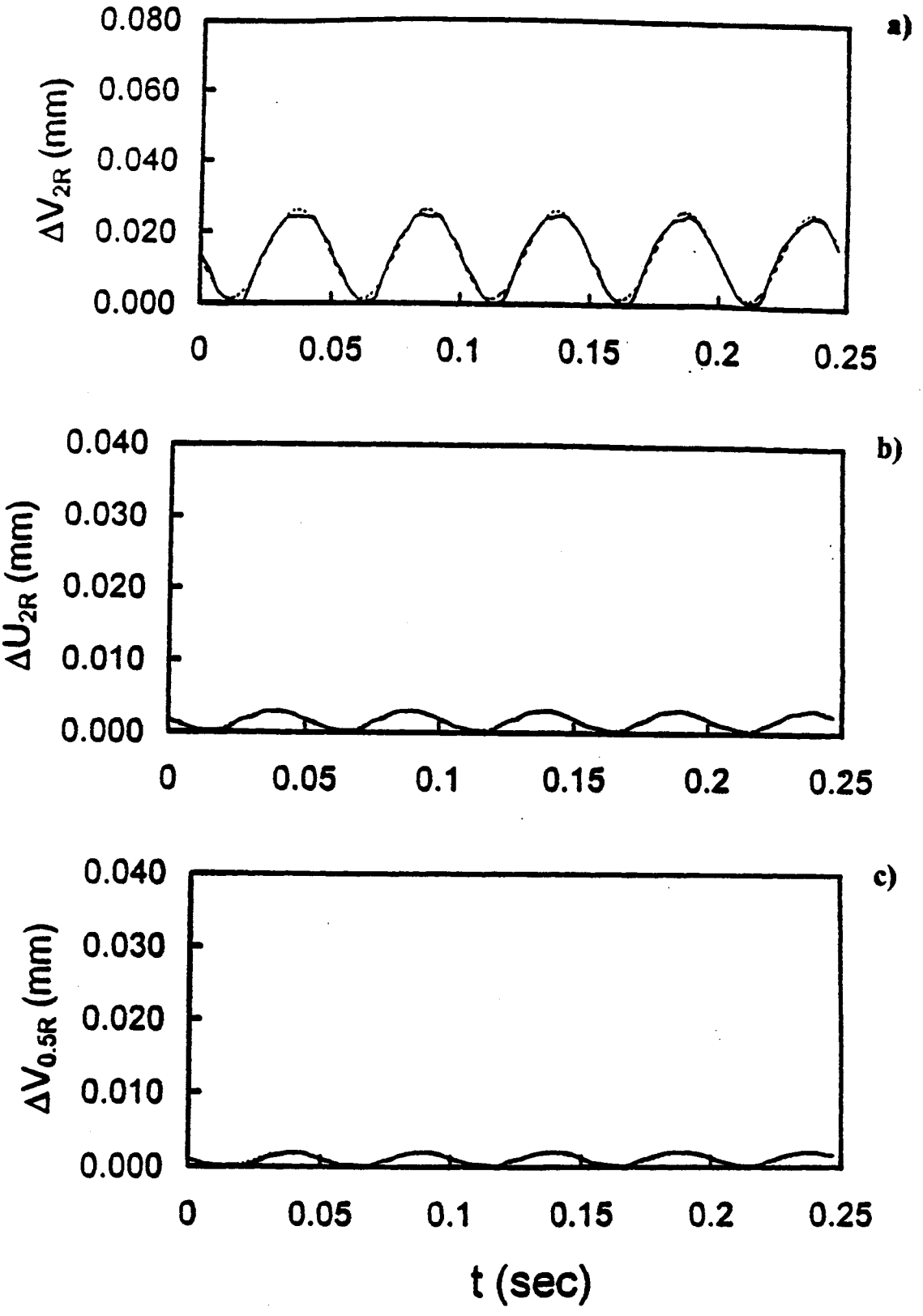

Fig. 15. Haversine test - B mixture, ω=20 Hz; a) change in length of vertical diameter, b) change in length of horizontal diameter, c) change in length of ¼ vertical diameter

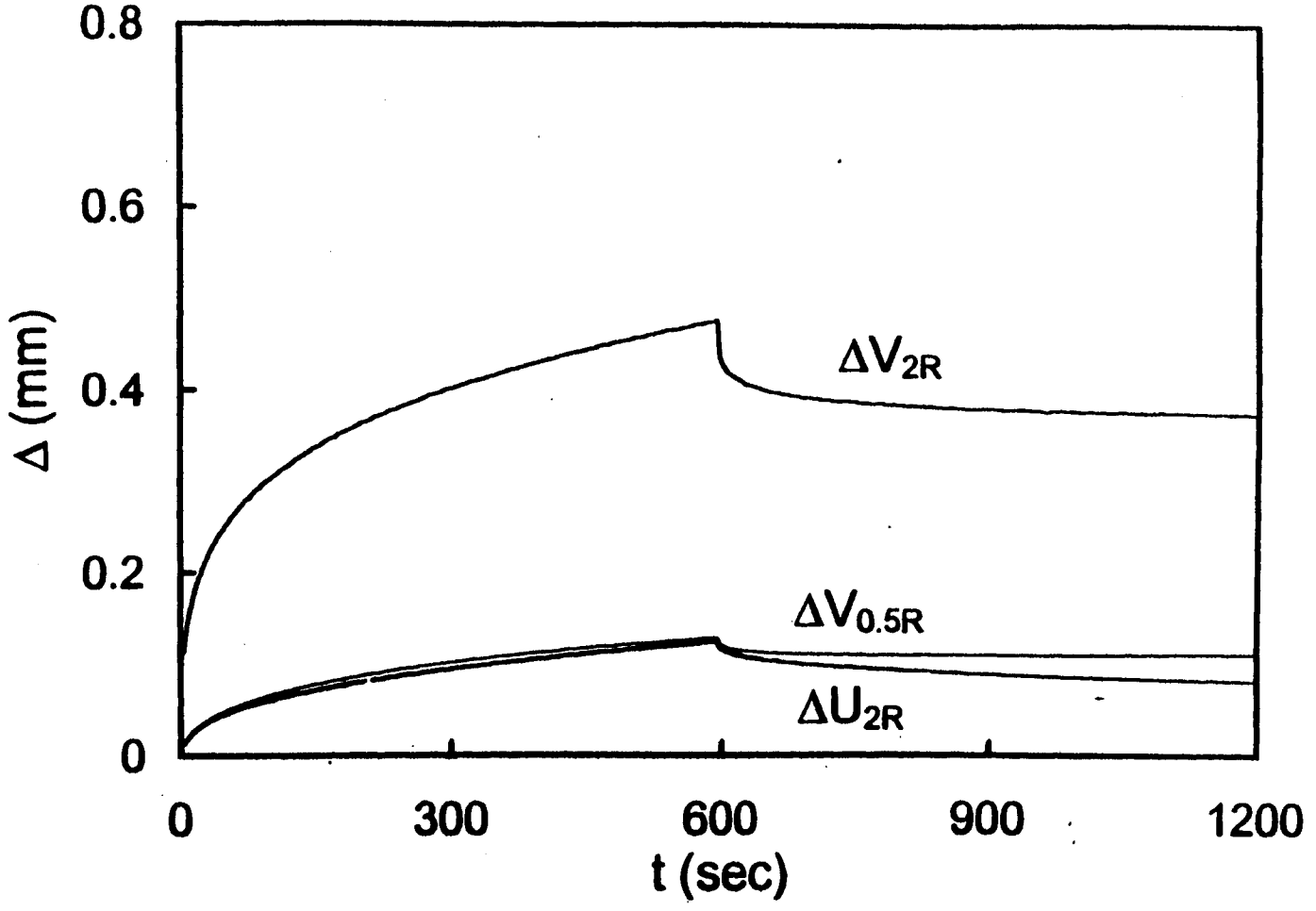

Fig. 16. Creep test - A mixture; change in length of vertical and horizontal diameters, and of ¼ of vertical diameter

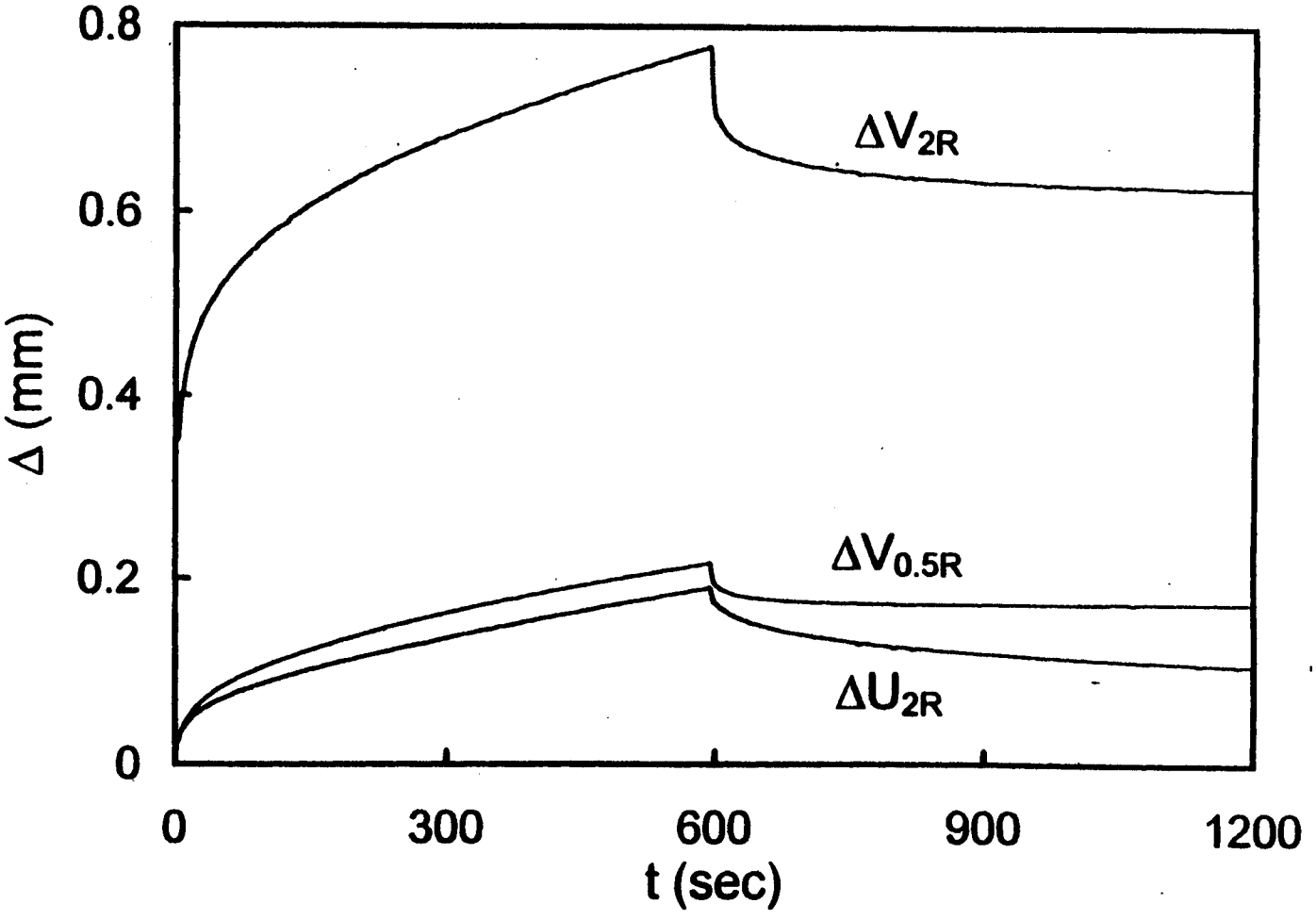

Fig. 17. Creep test - B mixture; change in length of vertical and horizontal diameters, and of ¼ of vertical diameter

Table 8. Group 2 Replicates

AC Type	Compactive Effort	Resilient Modulus	Haversine
-18°C (0°F)			
AC20 and 120/150 Pen	35 Blow	3	3
	50 Blow	3	3
	75 Blow	3	3
	Gyratory	3	3
1°C (34°F)			
AC20 and 120/150 Pen	35 Blow	3	3
	50 Blow	3	3
	75 Blow	3	3
	Gyratory	3	3
25°C (77°F)			
AC20 and 120/150 Pen	35 Blow	3	3
	50 Blow	3	3
	75 Blow	3	3
	Gyratory	3	3

CHAPTER 6

DATA ANALYSIS AND VISCOELASTIC PROPERTIES OF ASPHALT CONCRETE

In this chapter the results of Group 1 and Group 2 tests described in Chapter 5 are analyzed in the light of theoretical considerations presented in Chapters 3 and 4. In the analysis, the averaged results for each mixture were used; these were obtained by discarding the extreme results, and taking the average of the remaining ones.

GROUP 1 TESTS

Resilient Modulus Tests (Pulse/rest load)

Following the SHRP Protocol P07 procedure, the instantaneous and total resilient moduli and Poisson's ratios were determined from measurements of the change in length of the whole horizontal and vertical diameters, using Eqs (10) which are repeated below

$$E = \frac{0.27 + \nu}{\Delta U} \frac{P}{L} \tag{32a}$$

$$\nu = -3.59 \frac{\Delta U}{\Delta V} - 0.27 \tag{32b}$$

In addition, the Poisson's ratio was calculated from measurements of the change in length of the central, ¼ diameter vertical sector when Eq. (8b) becomes

$$\nu = \frac{-0.49\Delta U - 0.27\Delta V}{0.15\Delta U + \Delta V} \tag{33}$$

The results of calculations are presented in Table 9. It can be seen that for both mixtures the Poisson's ratios calculated using the measurements over the whole vertical diameter are

Table 9. Resilient Modulus and Poisson's Ratio

Frequency (Hz)	Mix A, ΔU_{2R}, ΔV_{2R} Total		Instantaneous	
	ν	E (MPa)	ν	E(MPa)
0.33	0.053	1933	0.044	2457
0.5	0.040	1982	0.030	2499
1.0	0.035	1974	0.024	2491
	Mix B, ΔU_{2R}, ΔV_{2R}			
0.33	0.185	1438	0.183	1894
0.5	0.181	1464	0.180	1927
1.0	0.182	1479	0.174	1947
	Mix A, ΔU_{2R}, $\Delta V_{0.5R}$			
0.33	0.290	3505	0.282	4527
0.5	0.273	3479	0.272	4520
1.0	0.273	3514	0.275	4622
	Mix B, ΔU_{2R}, $\Delta V_{0.5R}$			
0.33	0.397	2143	0.394	2796
0.5	0.380	2058	0.376	2710
1.0	0.349	2005	0.340	2652

substantially lower than 0.35, the value suggested for asphalt concrete at temperature 25 °C (77 °F) in ASTM D4123. The values of ν calculated using ΔV measured over the ¼ central sector, however, are much closer to 0.35. This result suggests that the change in length of the central vertical sector of the diameter provides more reliable data for evaluating material properties. The results listed in Table 9 also indicate that the Poisson's ratio of mixture A is lower than that of mixture B, and the resilient modulus of mixture A is greater than of mixture B. Considering the fact that mixture A was made of the stiffer binder, such results are expected.

Haversine Load Tests

The real and imaginary parts of the deviatoric and volumetric complex compliances were calculated using Eqs (30) of Chapter 4. In explicit form, when using the amplitudes of the change in length of the whole horizontal and vertical diameters, ΔU_0 and ΔV_0 (see Fig. 9), these equations become

$$J_{d1}(\omega) = (1.01\,\Delta U_0 \cos\delta_U + 0.20\,\Delta V_0 \cos\delta_V)\frac{L}{P_0} \tag{34a}$$

$$J_{d2}(\omega) = -(1.01\,\Delta U_0 \sin\delta_U + 0.20\,\Delta V_0 \sin\delta_V)\frac{L}{P_0} \tag{34b}$$

$$J_{v1}(\omega) = (0.43\,\Delta V_0 \cos\delta_U - 1.97\,\Delta U_0 \cos\delta_V)\frac{L}{P_0} \tag{34c}$$

$$J_{v2}(\omega) = -(0.43\,\Delta V_0 \sin\delta_U - 1.97\,\Delta U_0 \sin\delta_V)\frac{L}{P_0} \tag{34d}$$

and, when using the amplitudes of the change in length of the whole horizontal diameter and the central ¼ of the vertical diameter, they become

$$J_{d1}(\omega) = (0.74\,\Delta U_0 \cos\delta_U + 1.63\,\Delta V_0 \cos\delta_V)\frac{L}{P_0} \tag{35a}$$

$$J_{d2}(\omega) = -(0.74\,\Delta U_0 \sin\delta_U + 1.63\,\Delta V_0 \sin\delta_V)\frac{L}{P_0} \tag{35b}$$

$$J_{v1}(\omega) = (3.45\Delta V_0 \cos\delta_U - 2.54\,\Delta U_0 \cos\delta_V)\frac{L}{P_0} \tag{35c}$$

$$J_{v2}(\omega) = -(3.45\,\Delta V_0 \sin\delta_U - 2.54\,\Delta U_0 \sin\delta_V)\frac{L}{P_0} \tag{35d}$$

The results of calculations are plotted in Figs 18 to 25. It is seen that the volumetric response for mixture A is approximately frequency-independent; a similar result was found for mixture B. This means that viscosity plays a small role in the volumetric response to haversine loading, and the response can be assumed as purely elastic. It also is seen that the real and imaginary parts of the deviatoric complex compliance calculated using the amplitudes ΔV_0 of the whole vertical diameter are higher than those calculated using the amplitudes of the central ¼ sector. As higher value of compliance means softer response, the calculations based on the amplitudes ΔV_0 of the whole vertical diameter may underestimate the actual, stiffer material response.

Figure 26 depicts the deviatoric phase angle δ_d as a function of frequency, calculated from Eqs (35) and (20) using the amplitudes of the whole horizontal diameter, and the ¼ central sector of the vertical diameter. For both mixtures, upon small rise in the range of low frequencies, the phase angle gradually decreases when the frequency increases. The value of δ_d in the range of 20° to 40° indicates clearly the presence of viscosity in both mixtures; however, as anticipated by higher viscosity of binder in mixture A, this mixture is less viscous than mixture B.

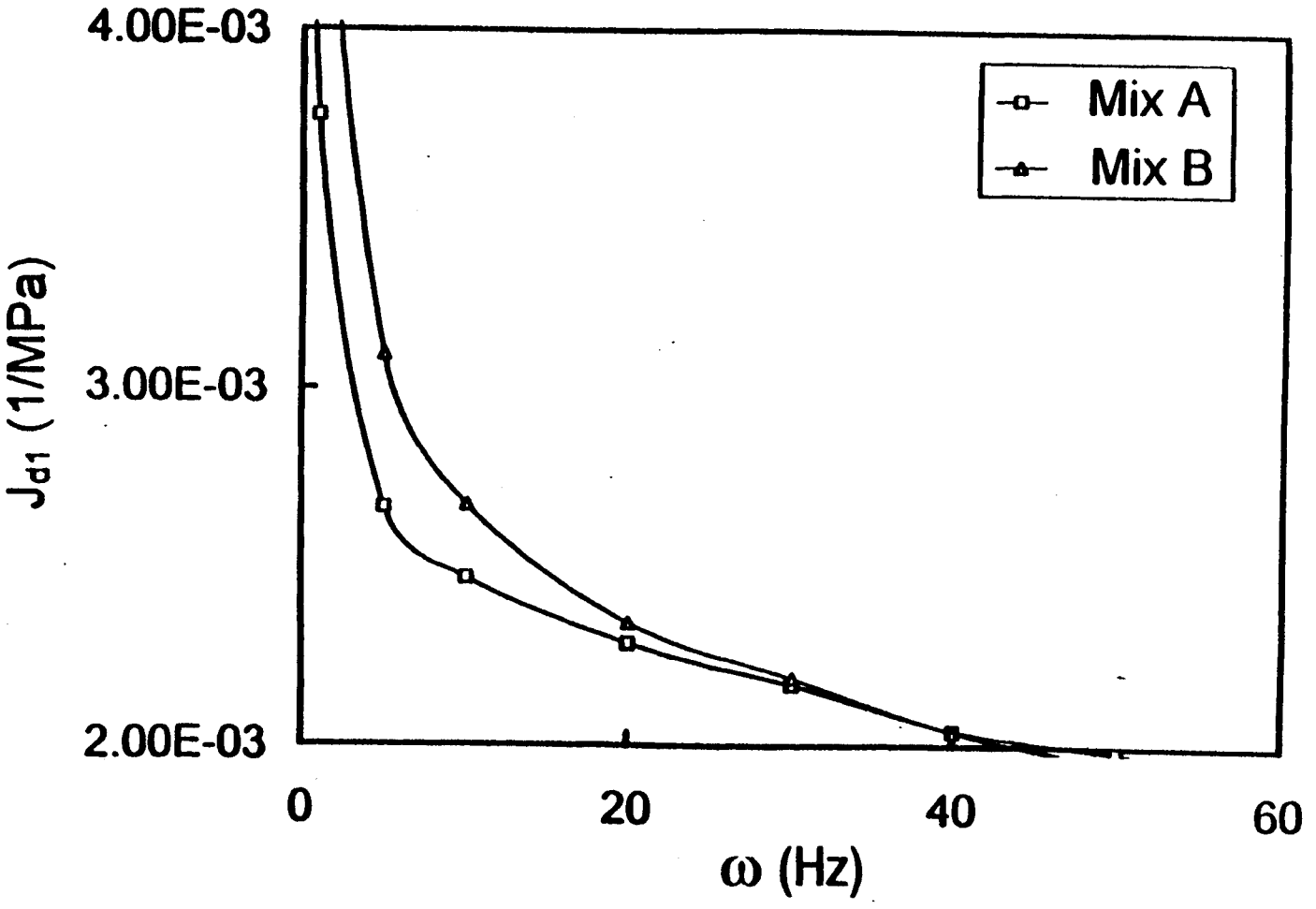

Fig. 18. Real part of deviatoric complex compliance determined from ΔU_{2R} and ΔV_{2R}

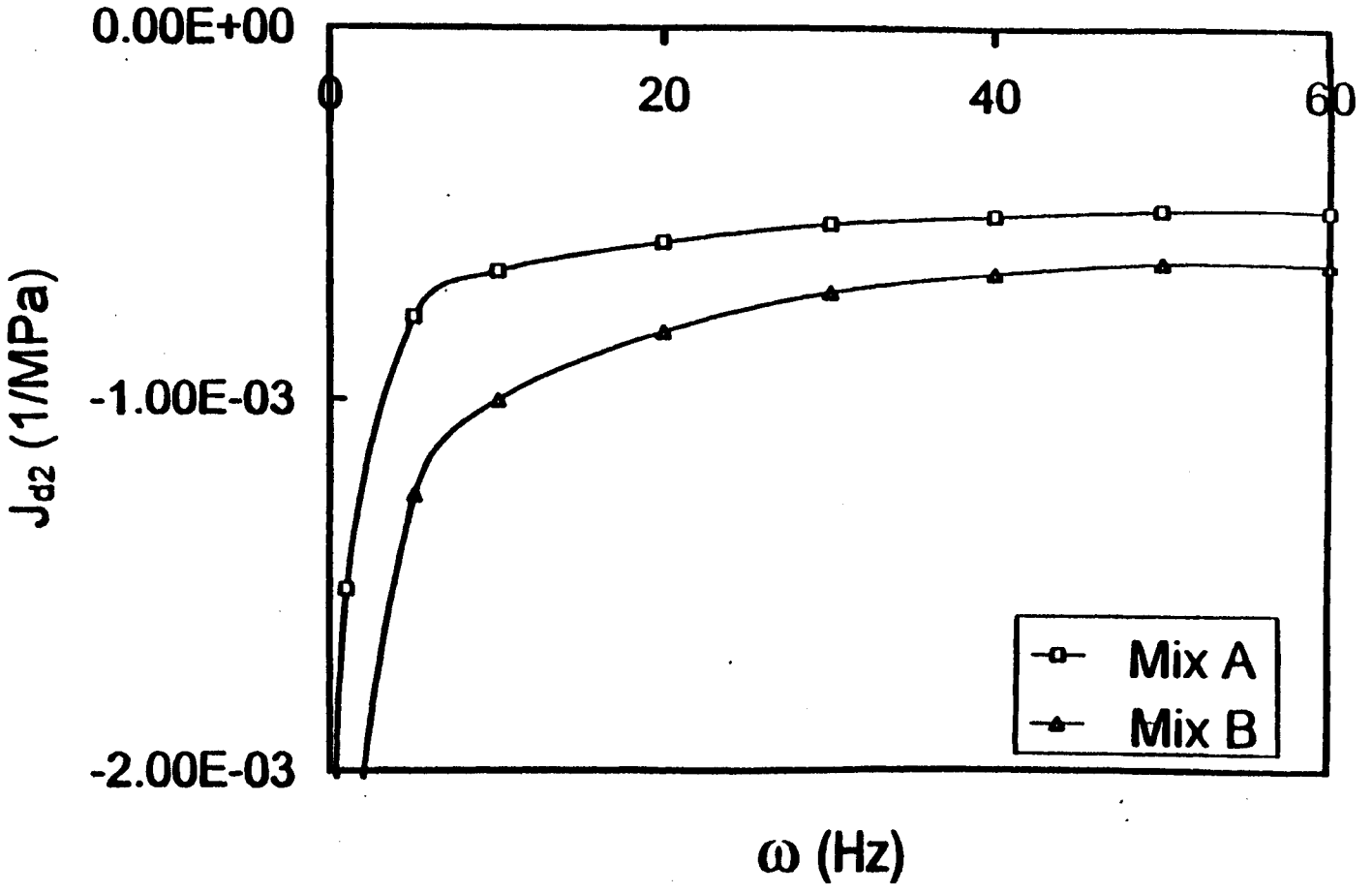

Fig. 19. Imaginary part of deviatoric complex compliance determined from ΔU_{2R} and ΔV_{2R}

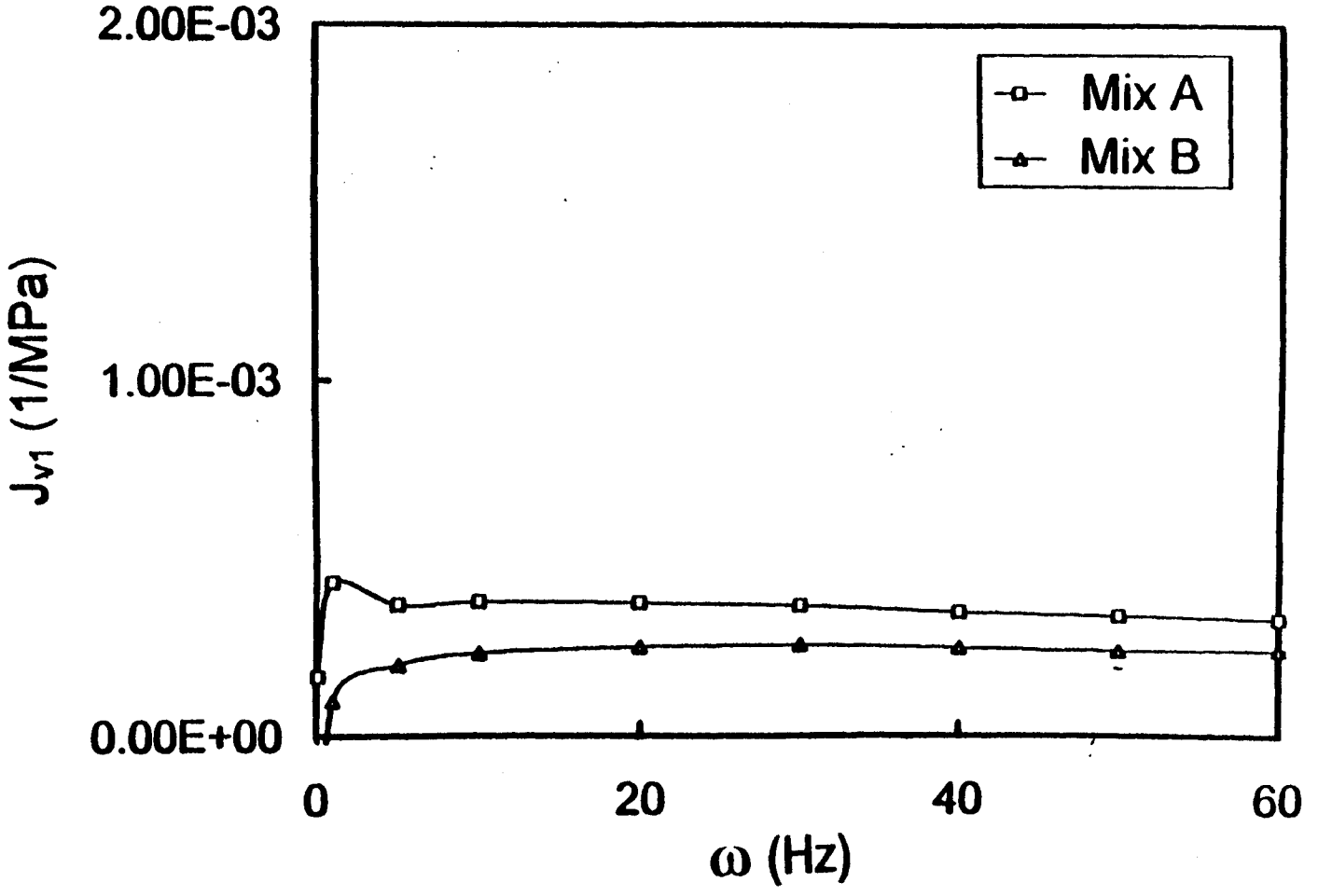

Fig. 20. Real part of volumetric complex compliance determined from ΔU_{2R} and ΔV_{2R}

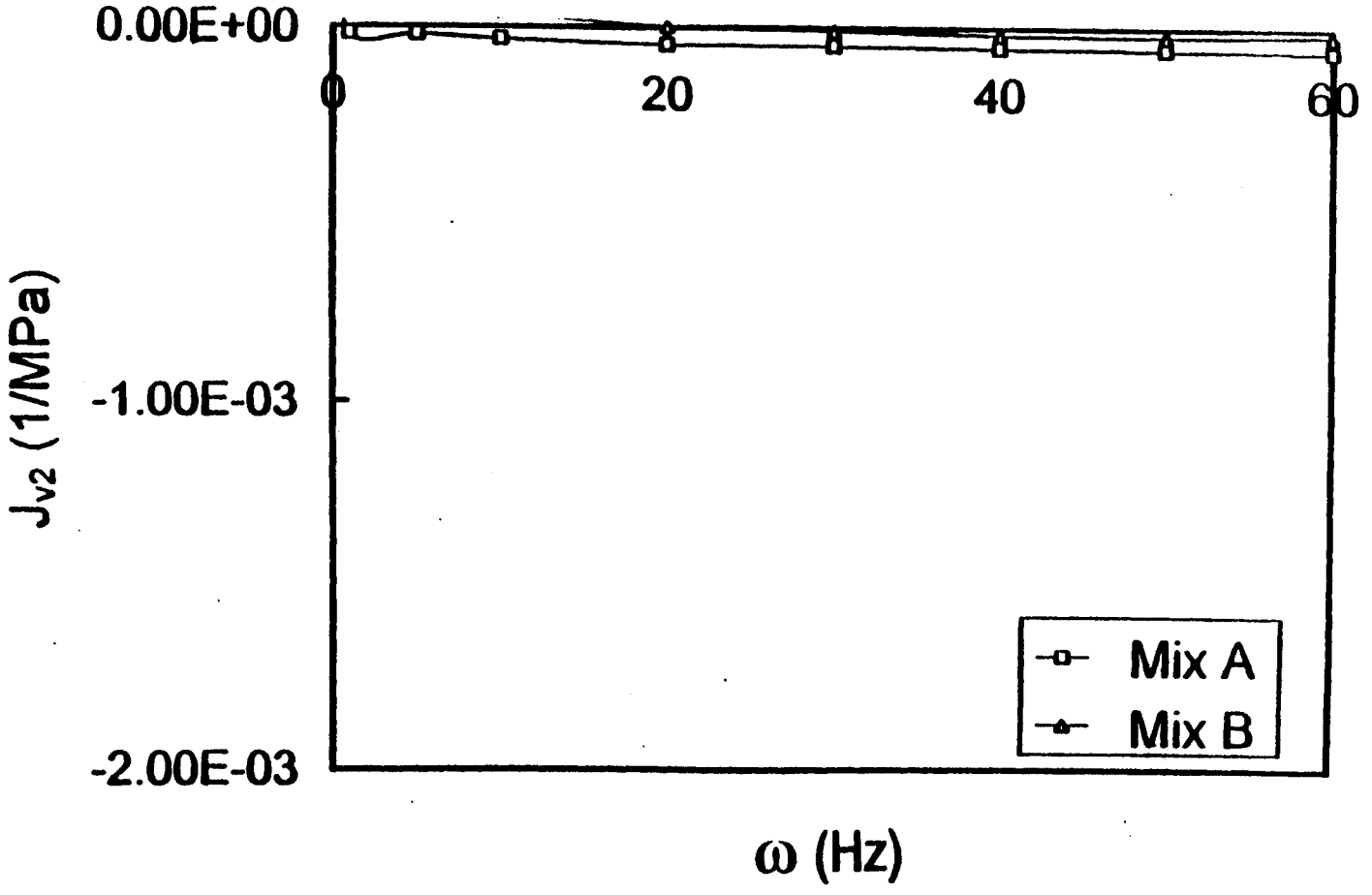

Fig. 21. Imaginary part of volumetric complex compliance determined from ΔU_{2R} and ΔV_{2R}

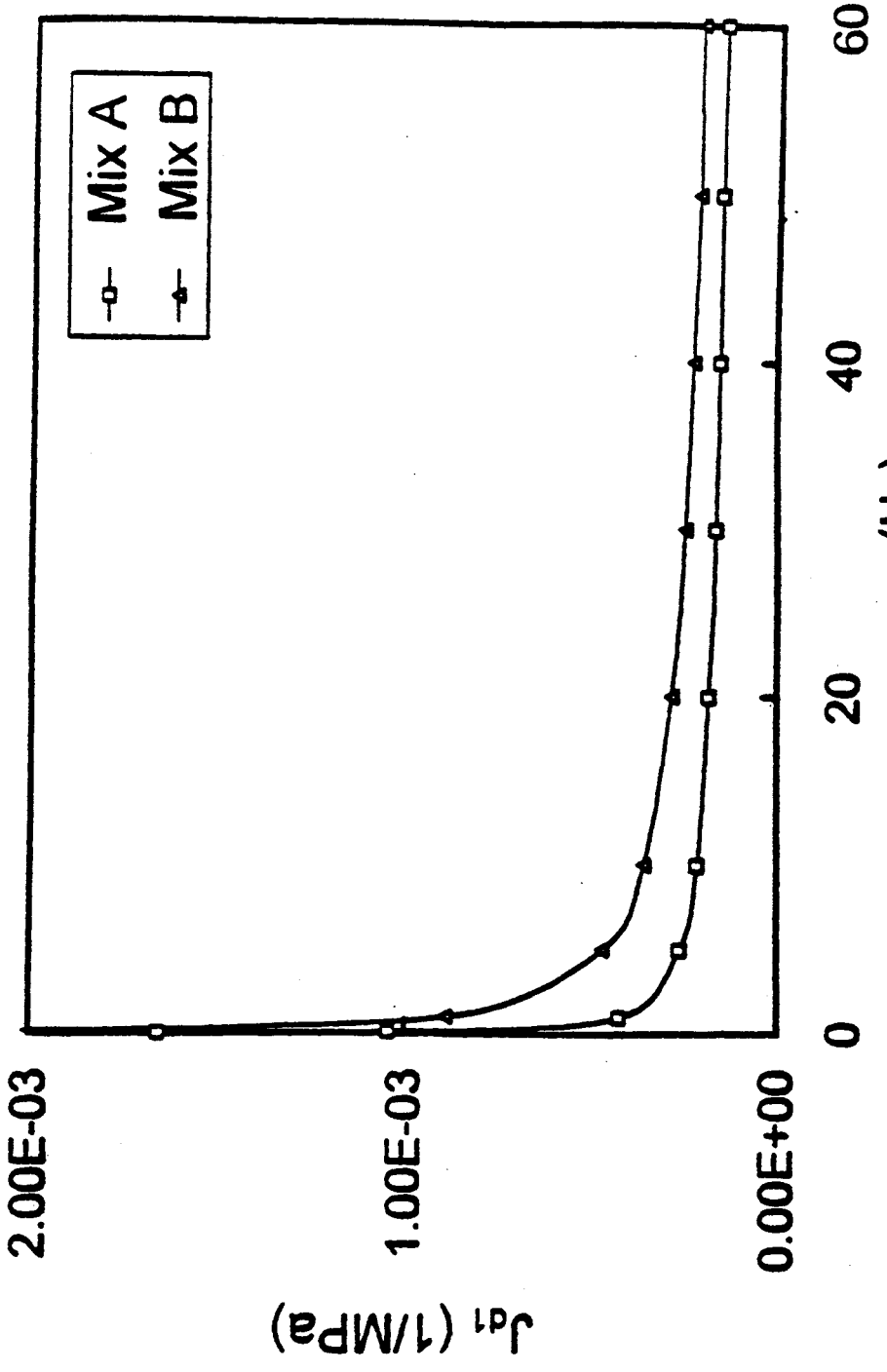

Fig. 22. Real part of deviatoric complex compliance determined from ΔU_{2R} and $\Delta V_{0.5R}$

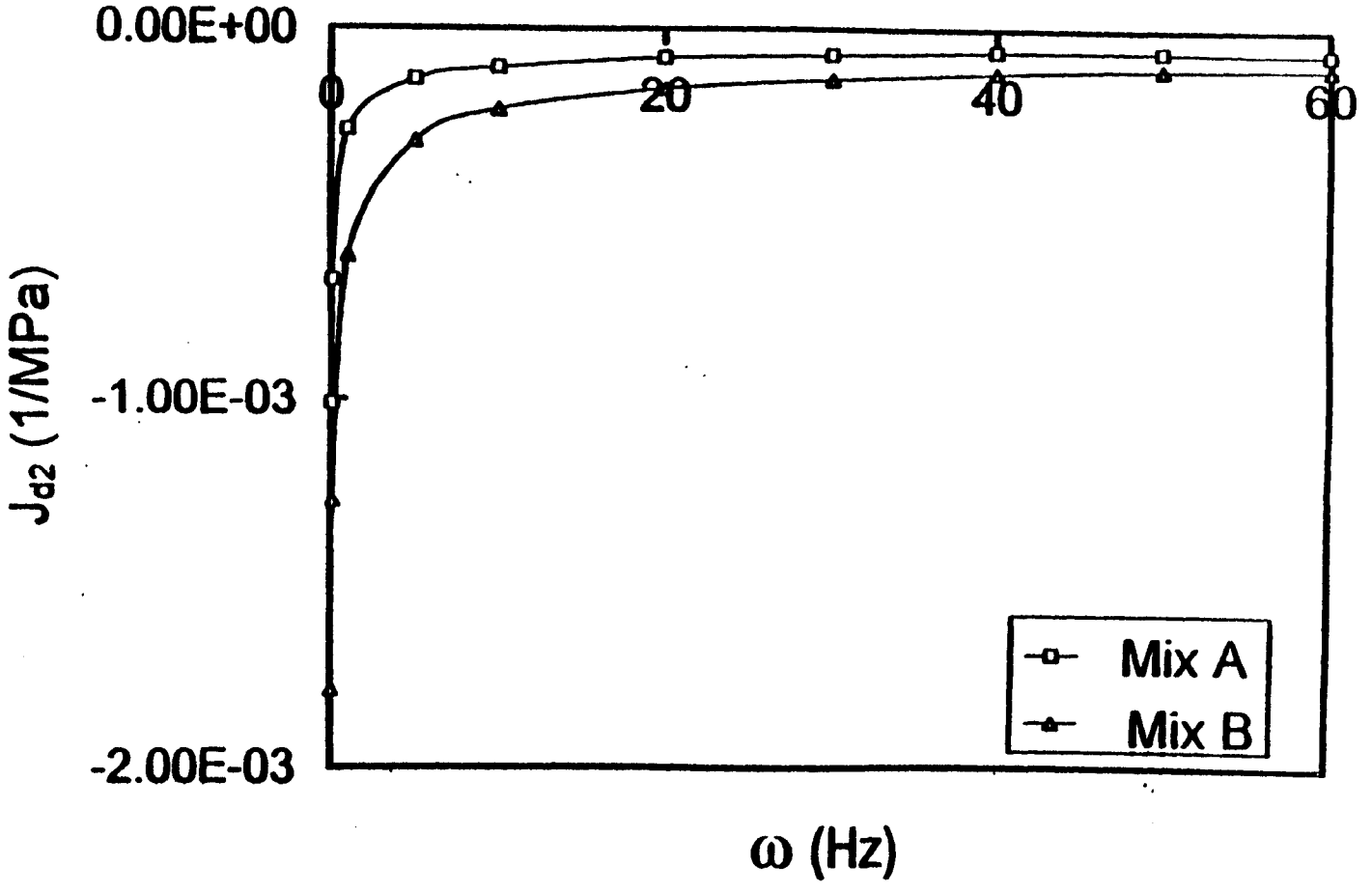

Fig. 23. Imaginary part of deviatoric complex compliance determined from ΔU_{2R} and $\Delta V_{0.5R}$

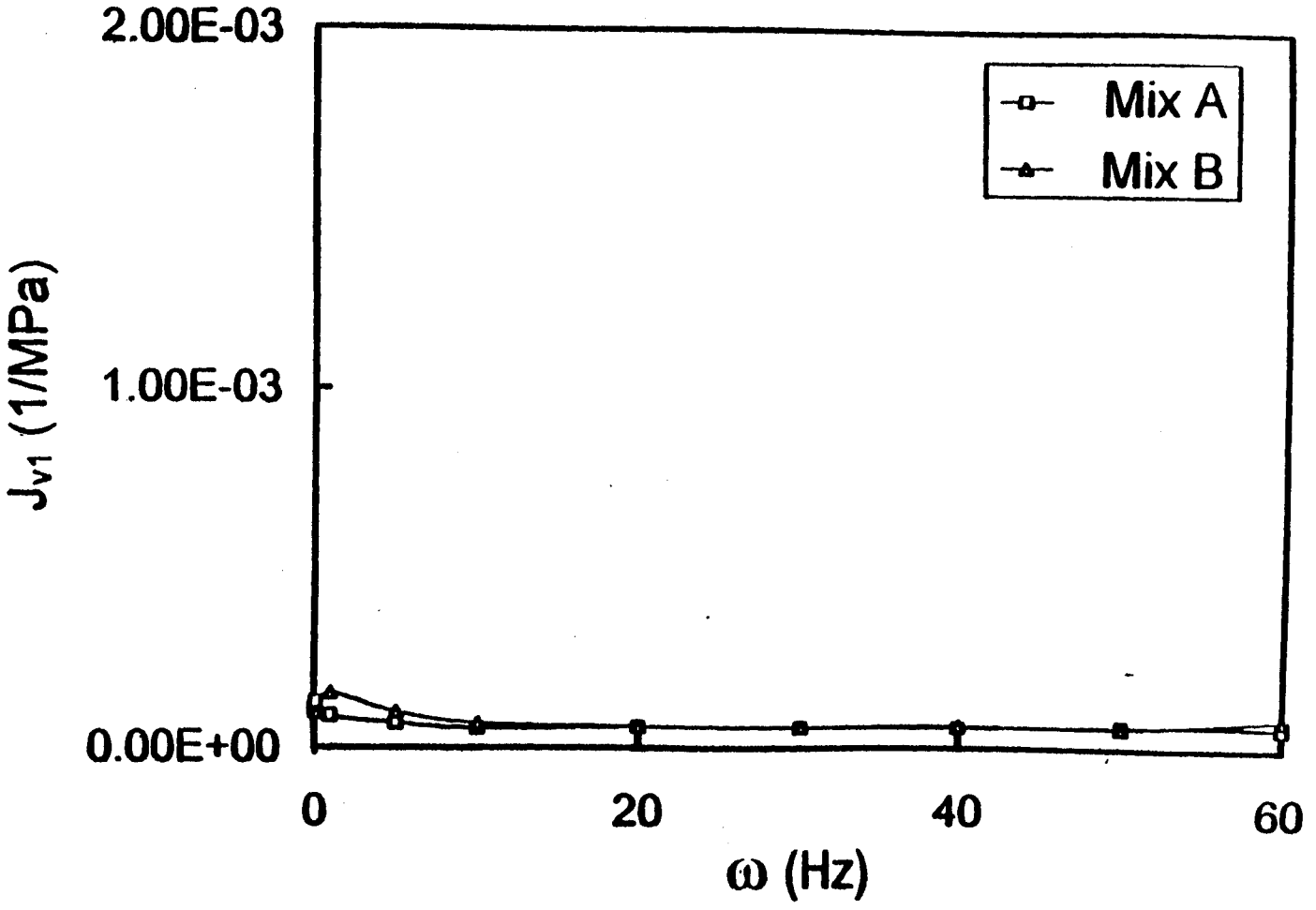

Fig. 24. Real part of volumetric complex compliance determined from ΔU_{2R} and $\Delta V_{0.5R}$

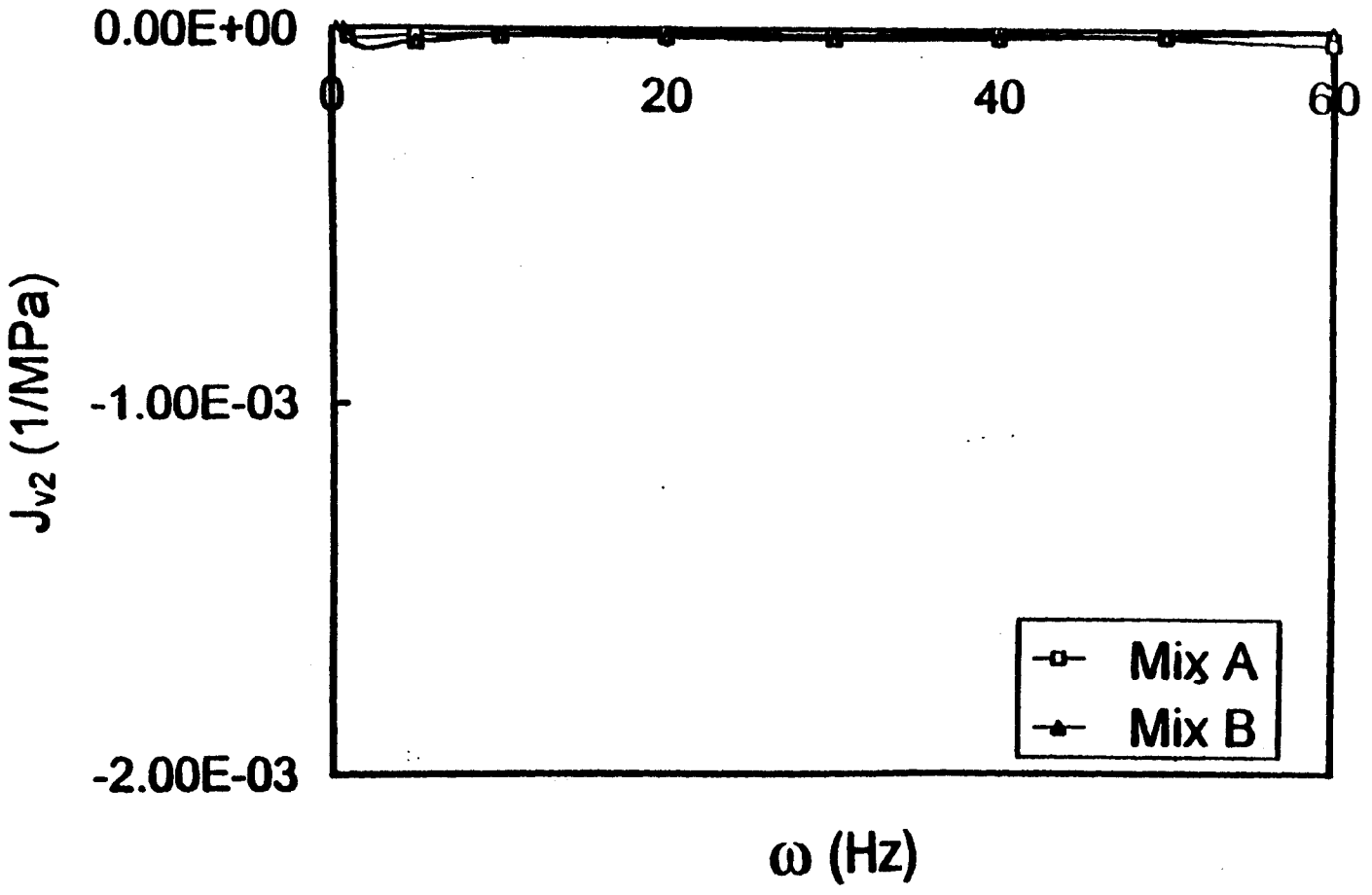

Fig. 25. Imaginary part of volumetric complex compliance determined from ΔU_{2R} and $\Delta V_{0.5R}$

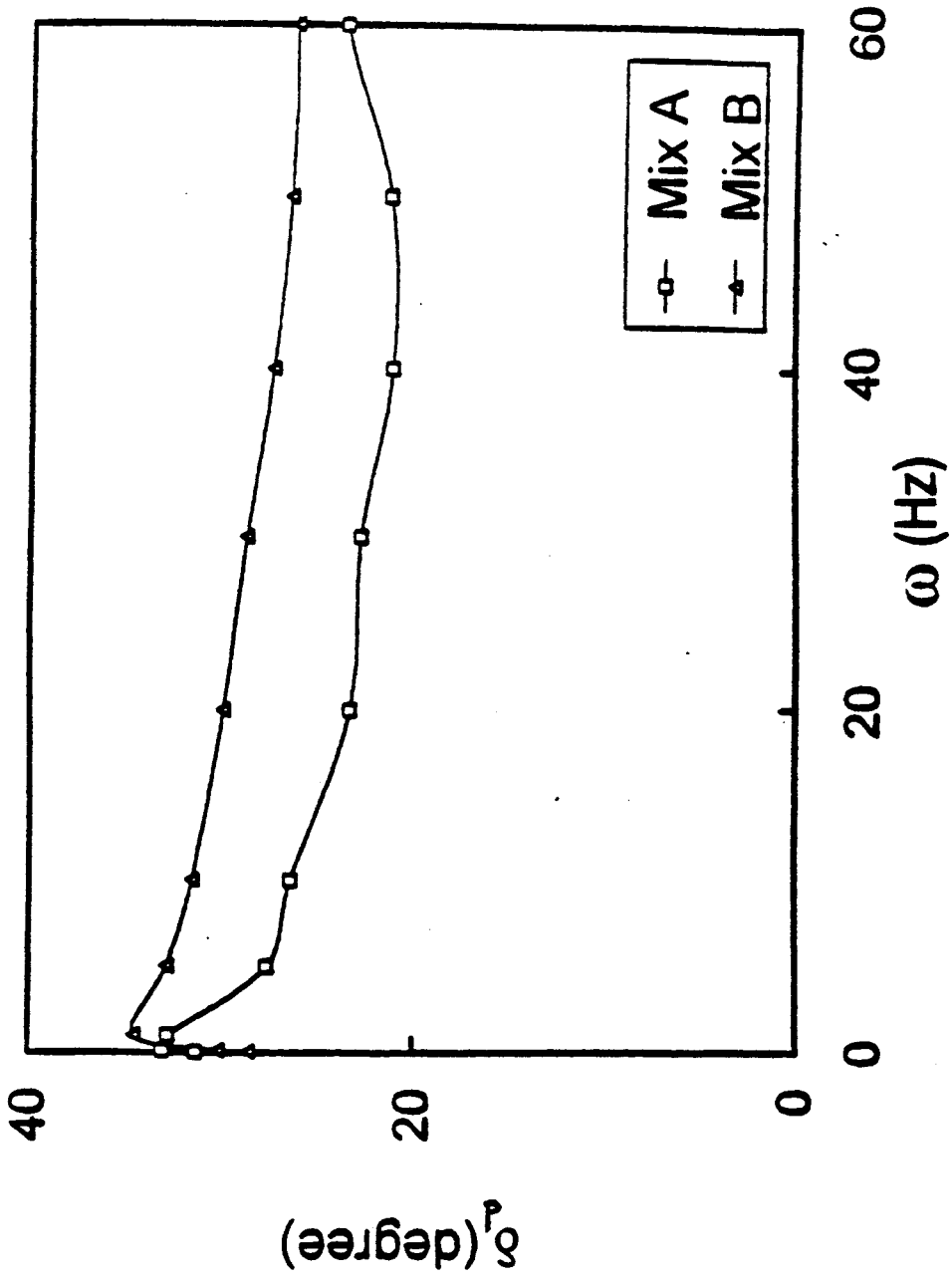

Fig. 26. Phase angle of deviatoric complex compliance determined from ΔU_{2R} and $\Delta V_{0.5R}$

Constant Load (Creep) Tests

The constant load (creep) test results were used to determine the deviatoric and volumetric creep compliance using the following expressions derived from Eqs (27) for ΔU measured over the whole horizontal diameter, and ΔV measured over the central, ¼ sector of the vertical diameter

$$J_d(t) = (0.74\Delta U - 1.63\Delta V)\frac{L}{P} \tag{36a}$$

$$J_v(t) = -(3.45\Delta U + 2.54\Delta V)\frac{L}{P} \tag{36b}$$

The appropriate values of ΔU and ΔV were determined from the rest period upon unloading, as the difference between the extended creep curves and recovery curves (see Fig. 8).

It was found, that the values of the volumetric compliances are very small and not very time-dependent, implying nearly purely elastic behavior. The deviatoric compliances, however, were time dependent as shown in Fig. 27. Clearly, mixture A less creeped than mixture B, and this is in agreement with haversine load test results described above.

GROUP 2 TESTS

Haversine Load Tests

The results of haversine load tests first were used to calculate the real and imaginary parts of the deviatoric and volumetric complex compliance using Eqs (35). Next, using Eqs (20), (21), and (22), the real and imaginary parts of the complex modulus, the magnitude of the complex compliance and modulus, and the phase angle all for the deviatoric response were calculated. These were not calculated for the volumetric response because of the low level of confidence in the volumetric complex compliance. The results of calculations are shown in Tables 10 and 11. It is seen that with increasing temperature the magnitude of the complex compliance $|J^*_d(\omega)|$ increases, and the magnitude of the complex modulus $|G^*_d(\omega)|$ it decreases. This can be anticipated, for

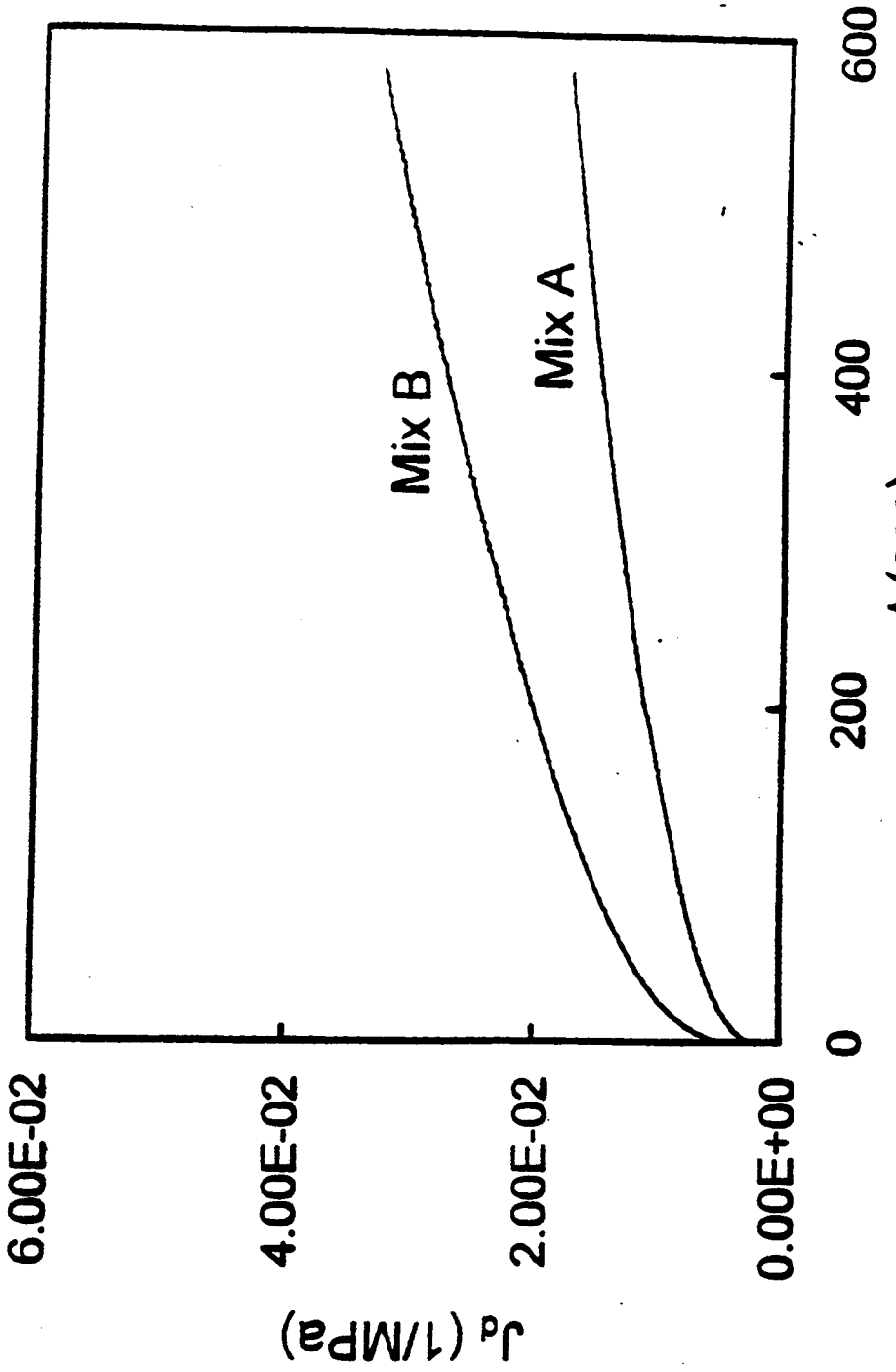

Fig. 27. Deviatoric creep compliance determine from recoverable ΔU_{2R} and $\Delta V_{0.5R}$

Table 10. Group 2 - Deviatoric Complex Compliances and Moduli, AC20, 0.1 Hz

Mix Design	$J_{d1}(\omega)$ MPa^{-1}	$J_{d2}(\omega)$ MPa^{-1}	$G_{d1}(\omega)$ MPa	$G_{d2}(\omega)$ MPa	$\lvert J_d^* \rvert$ MPa^{-1}	$\lvert G_d^* \rvert$ MPa	δ_d Degrees
-18°C							
35 Blow	3.82E-5	-6.43E-6	25,470	4,290	3.87E-5	25,830	9.57
50 Blow	—	—	—	—	—	—	—
75 Blow	—	—	—	—	—	—	—
Gyratory	—	—	—	—	—	—	—
1°C							
35 Blow	9.92E-5	-4.45E-5	8,740	3,850	1.09E-4	9,550	24.00
50 Blow	9.00E-5	-2.58E-5	10,430	3,180	9.39E-5	10,930	16.51
75 Blow	6.84E-5	-1.61E-5	14,090	3,610	7.05E-5	14,600	13.79
Gyratory	4.87E-5	-1.39E-5	19,000	5,430	5.06E-5	19,760	15.96
25°C							
35 Blow	6.45E-4	-4.94E-4	1,030	770	8.13E-4	1,280	37.22
50 Blow	5.01E-4	-4.00E-4	1,260	990	6.41E-4	1,600	38.37
75 Blow	4.98E-4	-3.76E-4	1,380	1,030	6.24E-4	1,720	36.95
Gyratory	3.15E-4	-2.02E-4	2,260	1,440	3.75E-4	2,680	32.57

Table 11. Group 2 - Deviatoric Complex Compliances and Moduli, AC20, 1.0 Hz

Mix Design	$J_{d1}(\omega)$ MPa^{-1}	$J_{d2}(\omega)$ MPa^{-1}	$G_{d1}(\omega)$ MPa	$G_{d2}(\omega)$ MPa	$\lvert J_d^* \rvert$ MPa^{-1}	$\lvert G_d^* \rvert$ MPa	δ_d Degrees
-18°C							
35 Blow	6.14E-5	-4.94E-6	16,180	1,300	6.16E-5	16,230	4.60
50 Blow	4.74E-5	-3.88E-6	21,880	1,640	4.76E-5	21,950	4.47
75 Blow	3.83E-5	-3.4E-6	30,740	2,670	3.84E-5	30,860	4.96
Gyratory	1.79E-5	-8.89E-7	55,580	2,750	1.80E-5	55,650	2.84
1°C							
35 Blow	7.33E-5	-1.24E-5	13,340	2,150	7.45E-5	13,530	9.38
50 Blow	6.59E-5	-1.09E-5	15,130	2,470	6.68E-5	15,332	9.30
75 Blow	5.15E-5	-8.37E-6	19,270	3,070	5.22E-5	19,520	9.15
Gyratory	2.73E-5	-2.98E-6	36,230	3,960	2.74E-5	36,440	6.24
25°C							
35 Blow	3.1E-4	-1.84E-4	2,450	1,430	3.61E-4	2,840	30.46
50 Blow	2.43E-4	-1.4E-4	3,140	1,790	2.81E-4	3,620	29.81
75 Blow	2.56E-4	-1.34E-4	3,210	1,660	2.89E-4	3,620	27.50
Gyratory	1.76E-4	-7.98E-5	4,730	2,140	1.93E-4	5,190	24.38

Table 12. Group 2 - Deviatoric Complex Compliances and Moduli, 120/150 Pen, 0.1 Hz

Mix Design	$J_{d1}(\omega)$ MPa^{-1}	$J_{d2}(\omega)$ MPa^{-1}	$G_{d1}(\omega)$ MPa	$G_{d2}(\omega)$ MPa	$\lvert J_d^* \rvert$ MPa^{-1}	$\lvert G_d^* \rvert$ MPa	δ_d Degrees
-18°C							
35 Blow	3.91E-5	-5.17E-6	25,150	3,330	3.94E-5	25,370	7.54
50 Blow	—	—	—	—	—	—	—
75 Blow	7.63E-5	-1.56E-6	13,100	268	7.63E-5	13,100	1.17
Gyratory	3.52E-5	-1.89E-6	28,360	1,530	3.52E-5	28,400	3.08
1°C							
35 Blow	1.83E-4	-7.75E-5	4,720	2,060	1.99E-4	5,160	23.25
50 Blow	1.9E-4	-7.09E-5	4,670	1,710	2.03E-4	4,970	20.28
75 Blow	1.52E-4	-5.96E-5	5,870	2,390	1.63E-4	6,340	21.84
Gyratory	1.16E-4	-4.53E-5	8,340	3,210	1.25E-4	9,940	21.20
25°C							
35 Blow	7.7E-4	-5.72E-4	930	700	9.6E-4	1,160	36.84
50 Blow	7.93E-4	-6.75E-4	740	630	1.04E-3	970	40.51
75 Blow	7.73E-4	-5.84E-4	820	630	9.70E-4	1,040	37.24
Gyratory	7.20E-4	-4.69E-4	1,020	670	8.6E-4	1,220	33.18

Table 13. Group 2 - Deviatoric Complex Compliances and Moduli, 120/150 Pen, 1.0 Hz

Mix Design	$J_{d1}(\omega)$ MPa^{-1}	$J_{d2}(\omega)$ MPa^{-1}	$G_{d1}(\omega)$ MPa	$G_{d2}(\omega)$ MPa	$\lvert J_d^* \rvert$ MPa^{-1}	$\lvert G_d^* \rvert$ MPa	δ_d Degrees
-18°C							
35 Blow	5.43E-5	-4.47E-6	18,940	1,550	5.44E-5	19,000	4.70
50 Blow	6.77E-5	-7.04E-6	15,370	1,750	6.81E-5	15,470	6.22
75 Blow	7.64E-5	-7.2E-6	29,350	5,020	7.68E-5	29,790	7.54
Gyratory	—	—	—	—	—	—	—
1°C							
35 Blow	1.20E-4	-3.98E-5	7,710	2,440	1.26E-4	8,100	17.97
50 Blow	1.24E-4	-3.38E-5	7,650	2,080	1.29E-4	7,930	15.22
75 Blow	9.86E-5	-2.68E-5	9,790	2,650	1.02E-4	10,140	15.20
Gyratory	8.68E-5	-2.15E-5	12,000	3,010	8.94E-5	12,370	13.99
25°C							
35 Blow	3.42E-4	-2.38E-4	2,240	1,500	4.17E-4	2,700	34.33
50 Blow	3.47E-4	-2.53E-4	1,910	1,400	4.3E-4	2,370	36.15
75 Blow	3.51E-4	-2.4E-4	1,960	1,350	4.25E-4	2,380	34.41
Gyratory	3.63E-4	-2.01E-4	2,210	1,240	4.15E-4	2,540	29.09

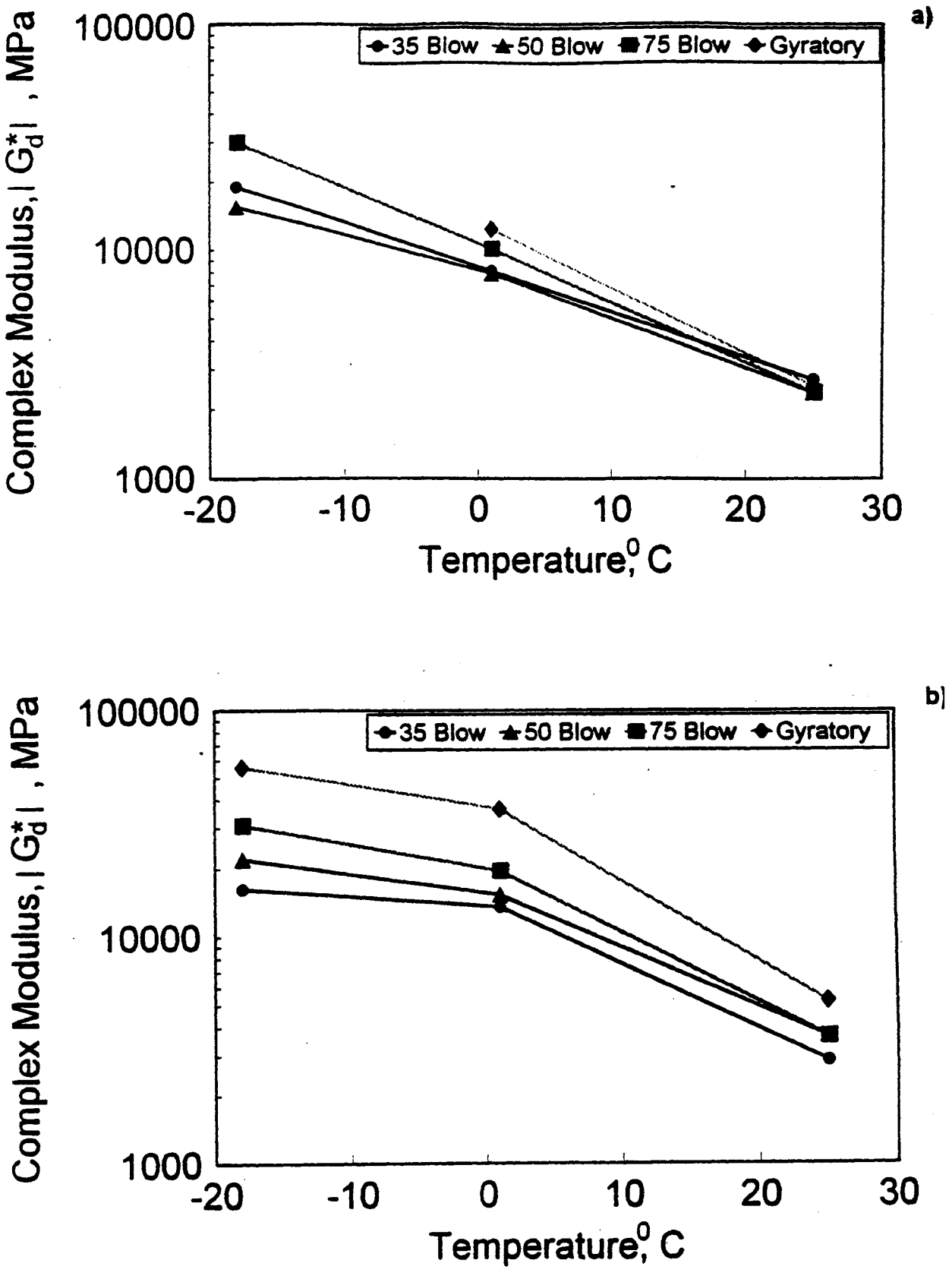

Fig. 28. Magnitude of deviatoric complex modulus *vs.* temperature

a) 120/150 Pen asphalt, ω=1.0 Hz, b) AC20 asphalt, ω=1.0

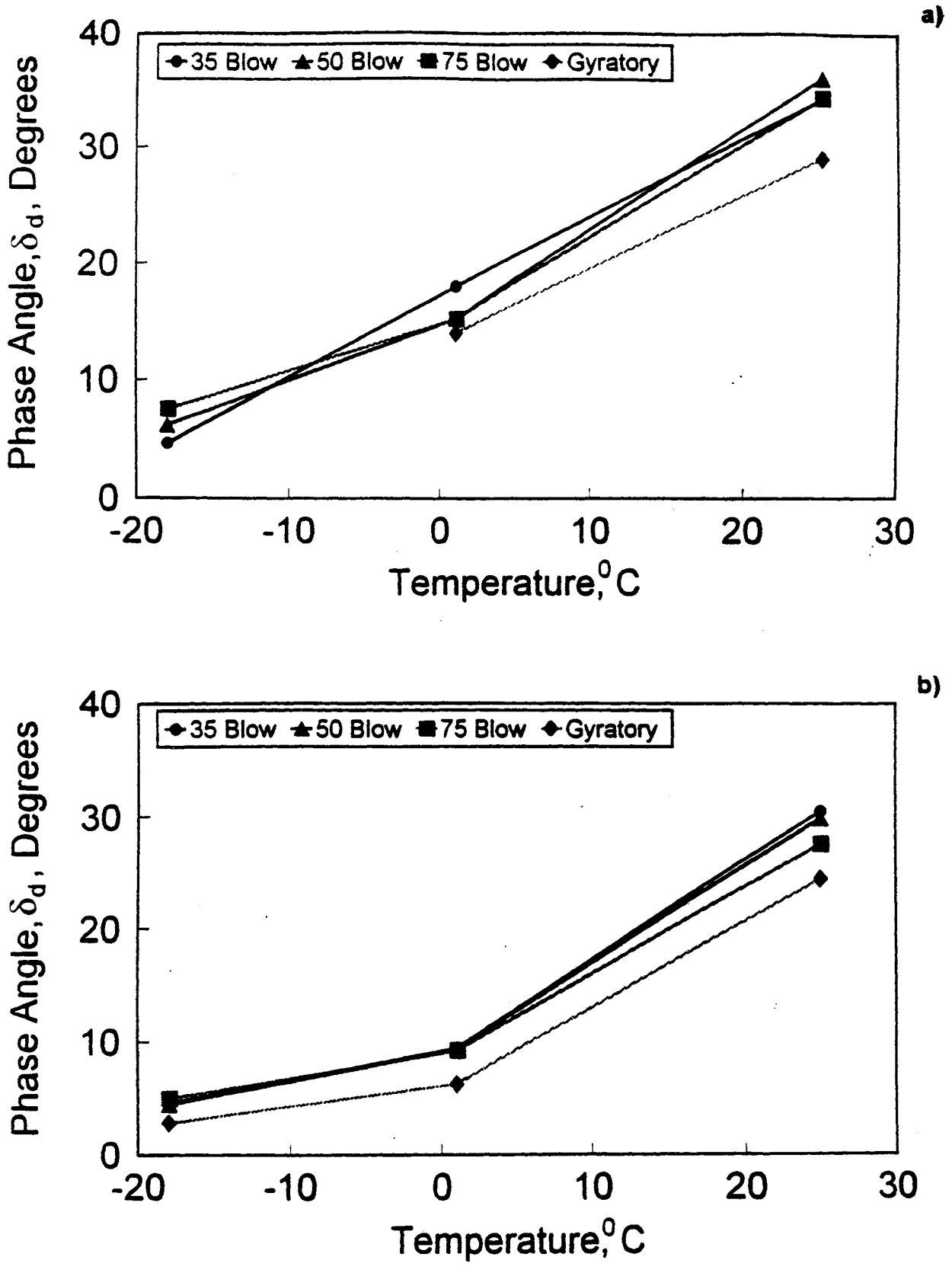

Fig. 29. Deviatoric phase angle *vs.* temperature

a) 120/150 Pen asphalt, ω=1.0 Hz, b) AC20 asphalt, ω=1.0 Hz

asphalt concrete becomes softer when heated. What seems more important is the presence of viscous effects even at the lowest temperature of -18 °C (0°F) as can be noted from the phase angle δ_d noticeably greater than zero. The influence of temperature on the magnitude of the deviatoric complex modulus and the deviatoric phase angle is clearly visible in Figs. 28 and 29.

Resilient Modulus Tests (Pulse/rest load)

Figure 30 shows the dependence of the total resilient modulus M_R on temperature. Likewise in the case of the magnitude of the complex modulus $|G^*_d(\omega)|$, the resilient modulus decreases with increasing temperature. When comparing Figs (28) and (30), however, it is seen that $|G^*_d(\omega)|$ is a more sensitive measure of temperature influence.

Although the numerical values of the resilient modulus M_R and the magnitude of the deviatoric complex modulus $|G^*_d|$ are not significantly different, there is no direct correlation between these two. The first quantifies stiffness of an elastic material, whereas the second of a viscoelastic material. Furthermore, M_R, equivalent to Young's modulus E, refers to combined deviatoric and volumetric response, and $|G^*_d|$ only to deviatoric (shear) response at a given frequency of load.

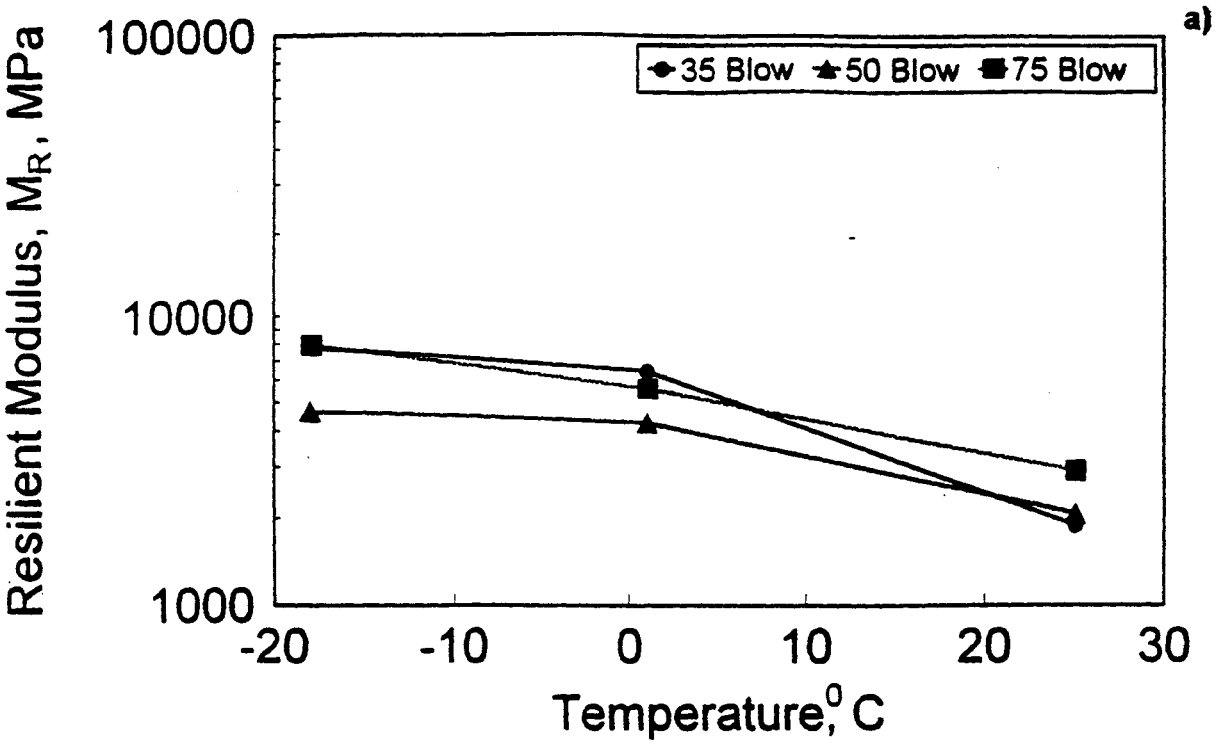

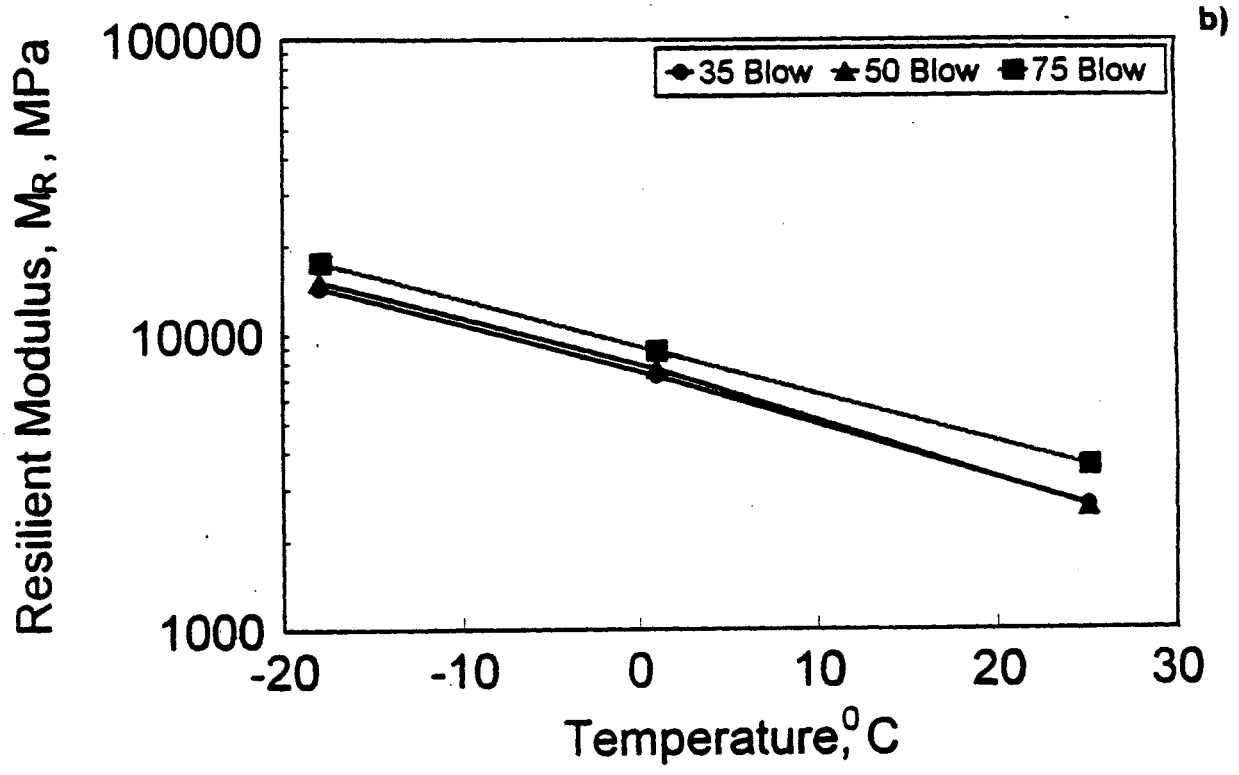

30. Resilient modulus *vs.* temperature

a) 120/150 Pen asphalt, ω=1.0 Hz, b) AC20 asphalt, ω=1.0 Hz

CHAPTER 7
CONCLUSIONS AND RECOMMENDATIONS

CONCLUSIONS

Based on the work described in previous chapters, the following conclusions can be drawn.

1. Measuring the change in length (deformation) of the whole vertical diameter of the specimen may lead to significant errors in evaluating the Poisson's ratio and the resilient modulus of asphalt concrete on the basis of elasticity theory. This also applies to evaluating the creep compliance and the relaxation modulus on the basis of viscoelasticity theory. Much more reliable results are obtained from measuring the deformation of the central, ¼ diameter, 25.4 mm (1 in.) long vertical sector. In the case of large-size aggregate, however, the 25.4 mm (1 in.) central sector may be too short, and a 50.8 mm (2 in.) sector may be necessary.

2. The resilient modulus and Poisson's ratio are not adequate measures of the viscoelastic properties of asphalt concrete. They should be regarded as valuable indices of overall material ability to deform and for material quality assessment rather than as mechanical parameters useful for predicting specific material response. For example, they cannot be used for evaluating cumulative material response to repeated or long-lasting loading conditions, which is the case of analyzing rutting, or for performing multilayer viscoelastic analysis of pavement systems.

3. In the case of traffic-induced periodic loading, the viscoelastic properties of asphalt concrete can be quantified by the complex compliance or modulus. The elastic properties can be quantified by the real part of the complex compliance or modulus. The viscous properties can be quantified by the imaginary part of the complex compliance or modulus or, more conveniently, by the phase angle. In addition, the overall deformability of asphalt concrete can be quantified by the magnitude of the complex compliance or complex modulus. All the

above quantities are well known and utilized in evaluating the viscoelastic properties of asphalt binders (AASHTO TP 5, in SHRP 1994).

4. A test which allows for determining the viscoelastic properties of asphalt concrete under traffic-induced periodic loading is the haversine load test. This test may provide means for a transition from resilient modulus testing for elastic behavior to the determination of viscoelastic properties of asphalt concrete. The haversine loading is somewhat easier to program and execute in most testing equipment than a pulse/rest scheme of loading.

5. The pulse/rest test recommended in ASTM D4123-82 and SHRP P07 Protocol is unsuitable for determination of the viscoelastic properties of asphalt concrete. This is because the data reduction process requires a non-linear regression algorithm with a high number of unknowns to be determined.

6. In the case of non-periodic loading, the viscoelastic properties of asphalt concrete can be quantified by the creep compliance or relaxation modulus. The creep compliance can be determined from constant load (creep) tests followed by a rest period.

7. The presence of viscous properties in asphalt concrete manifests itself in the deviatoric (shear) response, while the volumetric response is predominantly elastic. This is clearly visible by a deviatoric phase angle greater than zero, even at temperatures well below freezing.

8. Accurate measurements of the change in length (deformation) of the central, 25.4 mm (1 in.) vertical sector can be obtained by means of a clip-on displacement gage. However, the accuracy may decrease at temperatures higher than 25°C (77°F), when slip may occur in between the spacers and the specimen.

RECOMMENDATIONS

Based on the work described in previous chapters, the following recommendations are made.

1. The diametral compression haversine load test should be introduced as an appropriate test for determining the viscoelastic properties of asphalt concrete. Guidelines should be developed as to the load level, frequency range, and specific material parameter or function determination, e.g., phase angle, magnitude of complex modulus. Developing these guidelines will bring testing asphalt concrete in line with testing viscoelastic properties of asphalt binders (AASHTO TP 5, in SHRP 1994).

2. The role of the resilient modulus test as specified by the ASTM D4123-87 and SHRP Protocol P07 should be revised.

3. The vertical deformation of the cylindrical specimen should be measured over a central, shorter than the diameter sector of the specimen. A clip-on displacement gage developed in this research seems to provide accurate measurements over a 25.4 mm (1 in.) sector at low and moderate temperatures. An experimental program should be initiated to verify these findings, and establish temperature and measurement base limits for the gage satisfactory performance.

REFERENCES

AASHTO TP, (1994), Determining the Rheological Properties of Asphalt Binder Using a Dynamic Shear Rheometer (DSR), The SUPERPAVE Mix Design System Manual of Specifications, Test Methods and Practices.

ASTM Designation: D4123 - 82 (1987), Standard Test Method for Indirect Tension Test for Resilient Modulus Test of Bituminous Mixtures.

Berenbaum, R., and Brodie, I. (1959). "Measurement of the tensile strength of brittle materials." *Br.J.Appl.Phys.*, Vol.10, 281-286.

Blakey, F.A., and Beresford, F.D. (1955). "Tensile strains in concrete." CSIRO Div.Build.Res Rep. No.C2, 2-2, 15-31.

Drescher, A., Kim., Y., and Newcomb, D.E. (1993). "Permanent deformation in asphalt concrete." *J.Mat.Civ.Engrg., ASCE*, Vol.5, No.1, 112-128.

Fairhurst, C. (1964). "On the validity of the "Brazilian" test for brittle materials." *Int.J.Rock Mech.Min.Sci.*, Vol.1, 535-546.

Hadley, W.O., Hudson, W.R., and Kennedy, T.W. (1970). "A Method of Estimating Tensile Properties of Materials Tested in Indirect Tension." Research Report No.98-7, Center for Highway Research, University of Texas.

Hondros, G. (1959). "The evaluation of Poisson's ratio and the modulus of materials of a low tensile resistance by the Brazilian (indirect tensile) test with particular reference to concrete." *Austr.J.Appl.Sci.* Vol.10, 3, 243-268.

Jaeger, J.C. (1967). "Failure of rocks under tensile conditions." *Int.J.Rock Mech.Min.Sci.*, Vol.4, 219-227.

Livneh, M, and Shklarsky, E. (1962). "The splitting test for determination of bituminous concrete strength." *Proc. AAPT*, Vol.31, 457-476.

Lytton, R.L., Uzan, J., Fernando, E.G., Roque, R., Hiltunen, D., and Stoffels, S.M. (1993). "Development and validation of performance prediction models and specifications for

asphalt binders and paving mixes." SHRP-A-357.

Schmidt, R.J. (1972). "A Practical Method for Measuring the Resilient Modulus of Asphalt-Treated Mixes, " Highway Research Record 404, Highway Research Board, 22-32.

SHRP Protocol: P07, for SHRP Test Designation: AC07, Resilient Modulus for Asphalt Concrete, July, 1993.

Sousa, J.B., Taylor, R., and Tanco, A.J. (1991). "Analysis of some laboratory testing systems for asphalt-aggregate mixtures." Paper No.910743, presented at the 70th Annual Meeting of the Transportation Research Board, Washington, D.C.

Stroup-Gardiner, M. and Newcomb, D.E. (1996). "Investigation of Hot Mix Asphalt Mixtures at Mn/ROAD," Draft Final Report, Minnesota Department of Transportation, St.Paul.

Thaulow, S. (1957). "Tensile splitting test and high strength concrete test cylinders." *J.Amer. Concr.Inst.Proc.*, Vol.28, 53, 699-707.

Vinson, T.S. (1989). "Fundamentals of Resilient Modulus Testing," Workshop on Resilient Modulus Testing, State of the Practice, Oregon State University, Corvallis, March 28-30, 1989, .

Zhang, W. (1996). "Viscoelastic analysis of the diametral compression test on asphalt concrete." Ph.D. Thesis, University of Minnesota.

Zhang, W., Drescher, and Newcomb, D.E. (1996). "Viscoelastic behavior of asphalt concrete in diametral compression." *J.Transp.Engrg., ASCE*, (in press).

Zhang, W., Drescher, and Newcomb, D.E. (1996). "Viscoelastic analysis of diametral compression of asphalt concrete." *J.Eng.Mech., ASCE*, (in press).